Supplementary Information

Catalytic Reduction of Dinitrogen to Ammonia using Molybdenum Porphyrin Complexes

*Alexander S. Hegg,[1] Brandon Q. Mercado,[1] Alexander J. M. Miller,[2] Patrick L. Holland[1,]**

[1]Department of Chemistry, Yale University, New Haven, Connecticut 06511, United States

[2]Department of Chemistry, University of North Carolina at Chapel Hill, Chapel Hill, North Carolina 27599-3290, United States

*Corresponding author email: patrick.holland@yale.edu

Contents

General Considerations

All manipulations were performed under an atmosphere of N_2 gas in a M. Braun glovebox or on a Schlenk line unless otherwise specified. Unless otherwise noted, all solvents were dried via passage through Q5 columns from Glass Contour Co. and stored over molecular sieves prior to use. Deuterated solvents were degassed and dried over calcium hydride before storing over molecular sieves prior to use. Mesitaldehyde (Acros Organics, 97%), *p*-chloranil (Fluka, ≥97%), $BF_3{\cdot}OEt_2$ (Sigma, for synthesis), NEt_3 (Oakwood Chemical), $Mo(CO)_6$ (Aldrich, 98%), $TMSN_3$ (Millipore Sigma, 95%), ethylene glycol (Acros Organics, 99.8%), $[Ph_2NH_2][OTf]$ (Aldrich, 97%), decalin (Sigma Aldrich, mixture of cis- and trans- isomers, for synthesis) 1-chloronaphthalene (Sigma Aldrich, for synthesis), $HCl{\cdot}OEt_2$ (Sigma Aldrich, 2M in Et_2O), NaO^tBu (Strem Chemicals Inc., ≥98%), and TfOH (Aldrich, ≥99%) were used without further purification. Pyrrole (Sigma Aldrich, 98%) was dried with calcium hydride and distilled prior to use. SmI_2 (Sigma Aldrich, 99.9%) was purified by filtering a THF solution through Celite and evaporating solvent to give $SmI_2(THF)_2$. $[^nBu_4N][PF_6]$ (Alfa Aesar, 98%) was recrystallized from ethyl acetate and dried under vacuum prior to use. $TMPH_2$,[1] (TMP)MoN,[2] and $[HNEt_3][PF_6]$[3] were synthesized following reported procedures.

Instrumentation

NMR spectra were acquired on an Agilent 400 MHz spectrometer. ^1H NMR chemical shifts were referenced to residual ^1H signals from the deuterated solvent with which the sample was prepared.

UV-visible spectra were recorded on a Cary 60 spectrophotometer using resealable cuvettes with 1 mm path lengths.

IR spectra of solids or thin films were obtained using a Bruker Alpha spectrometer containing a diamond ATR unit with 2 cm^{-1} resolution.

Continuous-wave X-Band EPR spectra were recorded in perpendicular mode using a Bruker EleXsys EPR Spectrometer equipped with an ER 049X microwave bridge. The spectra were simulated using EasySpin.

Cyclic voltammetry was carried out with a CHI 660E potentiostat inside a nitrogen-filled glovebox in an undivided three-electrode cell which consisted of a 4 mm diameter glassy carbon working electrode, a Pt wire counter electrode, and an Ag wire reference electrode in a fritted sample holder separate compartment containing fresh electrolyte solution. An electrolytic solution of 0.2 M $[N^nBu_4][PF_6]$ in THF was used in all measurements, and an internal reference of ferrocene was included after initial data collection on the reference-free sample. The Randles-Sevcik equation (below) was used to determine the diffusion coefficient (D) for each porphyrin species. All of these coefficients were close to each other, showing only minor changes with metalation, oxidation state, or axial ligand identity.

$$i_p = 0.446nFAC^0\left(\frac{nFvD_0}{RT}\right)^{1/2}$$

In the Randles-Sevcik equation, i_p (A) is the peak current, v ($V{\cdot}s^{-1}$) is the square root of the scan rate, n is the number of electrons transferred in the redox event, A (cm^2) is the electrode surface area, D_0 ($cm^2{\cdot}s^{-1}$) is the diffusion coefficient of the analyte, and C^0 ($mol{\cdot}cm^{-3}$) is the bulk concentration of analyte

UV-Visible spectroelectrochemistry (UV-SEC) measurements were performed using a gas tight, optically transparent thin-layer solution cell (OTTLE cell) fabricated by Prof. Hartl at the University of Reading (Reading, U.K.), as described previously.[4] The OTTLE cell contained a masked Au-minigrid working electrode, a Pt-gauze auxiliary electrode, and an Ag-wire pseudo-reference electrode and had KBr windows. Analyte solutions were loaded directly into the OTTLE cell inside a nitrogen filled glovebox and the sealed cell was then brought outside the glovebox to perform the experiment. The potential of the cell was controlled by a CHI 660E potentiostat.

Ion chromatography (IC) was performed with a Metrohm 930 Compact IC Flex instrument equipped with a Metrosep C4–150/4.0 column for cation separation. A 1.75 mM oxalic acid solution was used as eluent. Samples for IC were prepared by dissolving solids in high purity water and filtered through a 0.45 μm syringe filter prior to analysis. A calibration curve was generated using standards from a commercial stock solution from (Metrohm, Custom Cation Mix:2). The MagIC Net software package was used to integrate the peaks of each chromatogram.

Gas chromatography (GC) analysis of the headspace of reaction mixtures was carried out on a ThermoFisher Scientific Trace 1300 gas chromatograph mol sieve 5Å PLOT capillary GC column (30 m length, 0.53 mm inner diameter, 30 μm average thickness) purchased from Sigma-Aldrich at 0.95 mL/min flow of N_2 carrier gas and a constant oven temperature of 35 ℃. Samples were detected using a TCD detector set to negative polarity.

Synthesis and Characterization of Compounds

(TMP)MoO (1): Synthesis followed the literature procedure until purification. After collecting purple precipitate from the cooled reaction mixture, this material was loaded onto a Celite plug. Remaining free-base ligand was removed by washing with pentane, then the product was flushed through with toluene. Crystals suitable for X-ray diffraction were grown from diffusion of pentane (3:1) into a concentrated toluene solution of the product at −35 °C over several days. This gave the product in 60% yield. **^{1}H NMR** (400 MHz, C_6D_6): δ 9.07 (s, 8H, β-pyrrole), 7.13 (s, 4H, *m*-aryl), 7.11 (s, 4H, *m*-aryl), 2.43 (s, 12H, *p*-methyl), 1.94 (s, 12H, *o*-methyl), 1.73 (s, 12H, *o*-methyl) ppm. **FT-IR** (solid, cm^{-1}): 2963 (w), 2912 (s), 2847 (s), 2730 (w), 1874 (m), 1825 (w), 1609 (w), 1576 (m), 1542 (w), 1444 (s), 1407 (w), 1376 (m), 1360 (w), 1344 (w), 1323 (m), 1299 (w), 1203 (m), 1189 (w), 1062 (w), 1005 (s), 977 (s), 946 (m), 848 (m), 830 (m), 803 (s), 767 (w), 726 (s), 708 (m), 689 (m), 665 (w), 622 (w), 602 (w), 559 (m), 432 (w) cm^{-1}. **UV-vis** (CH_2Cl_2, ε in mM^{-1} cm^{-1}): 431 nm (207), 554 nm (11), and 641 nm (4.2).

(TMP)MoCl$_2$ (2): In a 100 mL Schlenk flask equipped with a magnetic stir bar, (TMP)MoO (0.2582 g, 0.2885 mmol) was dissolved in 25 mL of toluene under an N_2 atmosphere. To the stirring mixture $HCl{\cdot}OEt_2$ (2M, 15.0 mL, 30.0 mmol) was added via syringe, and the reaction was stirred at room temperature. The red solution quickly turned green and solid precipitate was visible in solution. After 2 hours, volatile materials were removed under vacuum, leaving dark green solids. The solids were loaded onto a Celite plug. The material was rinsed with pentane until rinses were clear, removing a red solution containing residual **1** and $TMPH_2$. The residue was flushed through the plug using CH_2Cl_2 until rinses were clear (about 75 mL). The volatile components of the mixture were removed with vacuum, yielding **2** as a green solid (0.156 g, 57%). Crystals suitable for X-ray diffraction were grown from a 3:1 layering of pentane and a concentrated solution of **2** in CH_2Cl_2 at –35 °C overnight (47%). **^{1}H NMR** (400 MHz, C_6D_6): δ 17.28 (s, 8H, β-pyrrole), 6.80 (s, 8H, *m*-aryl), 2.41 (s, 12H, *p*-methyl), 1.81 (s, 24H, *o*-methyl) ppm. **Evans** (C_6D_6,

295 K): μ_{eff} = 2.1 μB. **FT-IR** (solid, cm^{-1}): 2995 (w), 2971 (w), 2951 (w), 2914 (m), 2855 (w), 1609 (w), 1544 (w), 1523 (w), 1511 (w), 1493 (m), 1440 (m), 1376 (m), 1313 (w), 1189 (m), 1154 (w), 1060 (w), 1030 (w), 1005 (s), 960 (m), 950 (m), 938 (m), 899 (w), 865 (m), 850 (m), 826 (w), 805 (s), 732 (s), 724 (s), 693 (s), 620 (w), 612 (w), 604 (w), 597 (w), 559 (m), 518 (w), 463 (m), 424 (m), 412 (w) cm^{-1}. **UV-vis** (CH_2Cl_2, ε in cm^{-1} mM^{-1}): 359 nm (38), 378 nm (36), 456 nm (9.3), 513 nm (6.8) and 592 nm (4.0).

(TMP)MoN (3): We followed the synthetic method in ref. 2, which worked even though the starting material was misassigned as (TMP)Mo but is actually (TMP)MoO. **FT-IR** (solid, cm^{-1}): 2963 (w), 2948 (w), 2914 (w), 2853 (w), 1609 (w), 1590 (w), 1564 (w), 1503 (w), 1472 (w), 1431 (m), 1378 (m), 1327 (m), 1299 (w), 1250 (w), 1201 (m), 1158 (w), 1138 (w), 1060 (m), 1036 (m), 1011 (s), 967 (s), 911 (w), 867 (m), 854 (m), 830 (s), 791 (s), 767 (s), 738 (m), 724 (s), 663 (s), 640 (w), 559 (m), 538 (s), 514 (w), 428 (w), 408 (w) cm^{-1}. **UV-vis** (toluene, ε in cm^{-1} M^{-1}): 410 (5.67×10^4), 433 (5.32×10^5), 562 (2.67×10^4), 600 (1.76×10^4).[2]

$TMPH_2$: Synthesis according to literature procedures,[1] crystallized from concentrated CH_2Cl_2 solution in methanol. **^{1}H NMR** (400 MHz, C_6D_6): δ 8.81 (s, 8H, β-pyrrole), 7.13 (s, 8H, *m*-aryl), 2.42 (s, 12H, *p*-methyl), 1.89 (s, 24H, *o*-methyl), -1.63 (s, 2H, NH) ppm. **FT-IR** (solid, cm^{-1}): 3318 (w), 2948 (m), 2914 (m), 2853 (m), 1611 (w), 1558 (m), 1468 (s), 1450 (m), 1401 (m), 1376 (m), 1344 (m), 1211 (m), 1189 (m), 1152 (w), 1060 (w), 1044 (w), 1032 (w), 1013 (w), 991 (m), 979 (m), 969 (s), 944 (s), 909 (w), 850 (m), 826 (w), 801 (s), 771 (w), 734 (s), 720 (s), 695 (m), 683 (w), 675 (w), 642 (w), 559 (m), 426 (w) cm^{-1}.

NMR Spectra

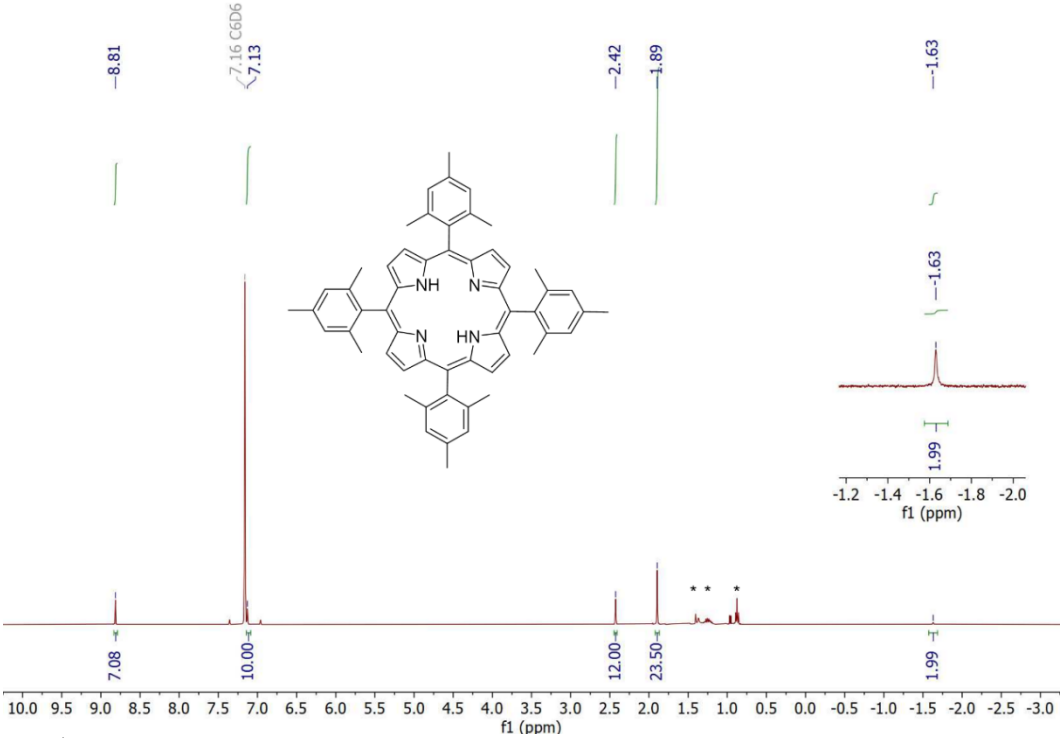

Figure S1: ^{1}H NMR spectrum of $TMPH_2$ in C_6D_6. Pentane and grease impurities are marked with *. An inset shows the pyrrole N-H peak at -1.63 ppm.

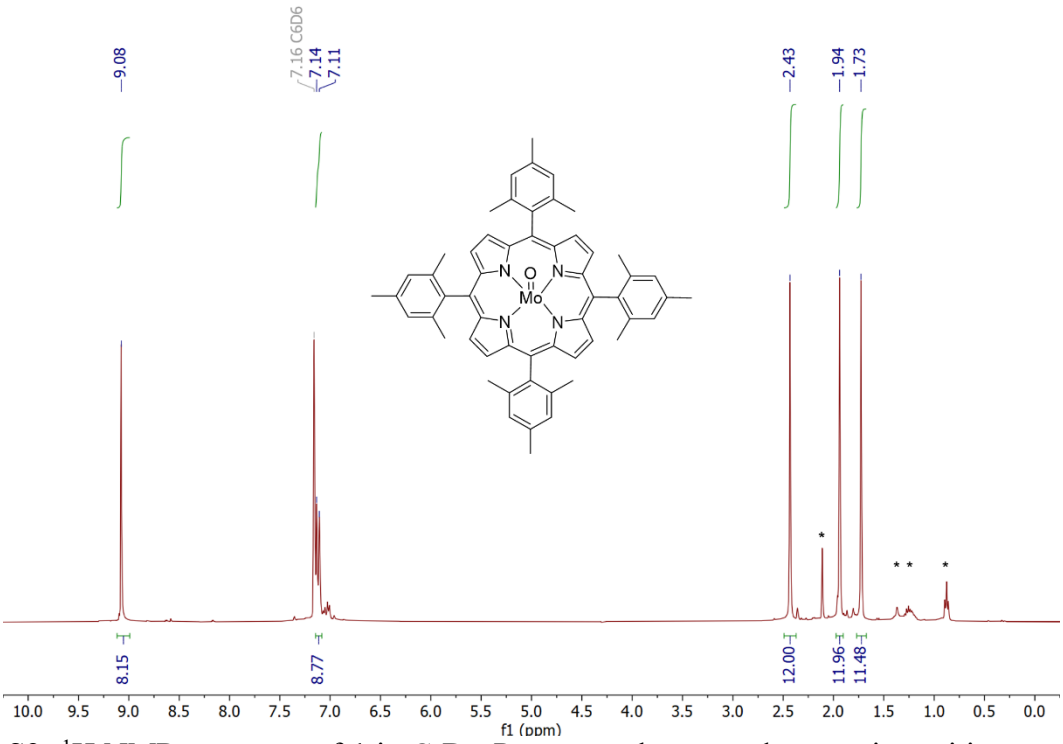

Figure S2: ^{1}H NMR spectrum of **1** in C_6D_6. Pentane, toluene, and grease impurities are marked with *.

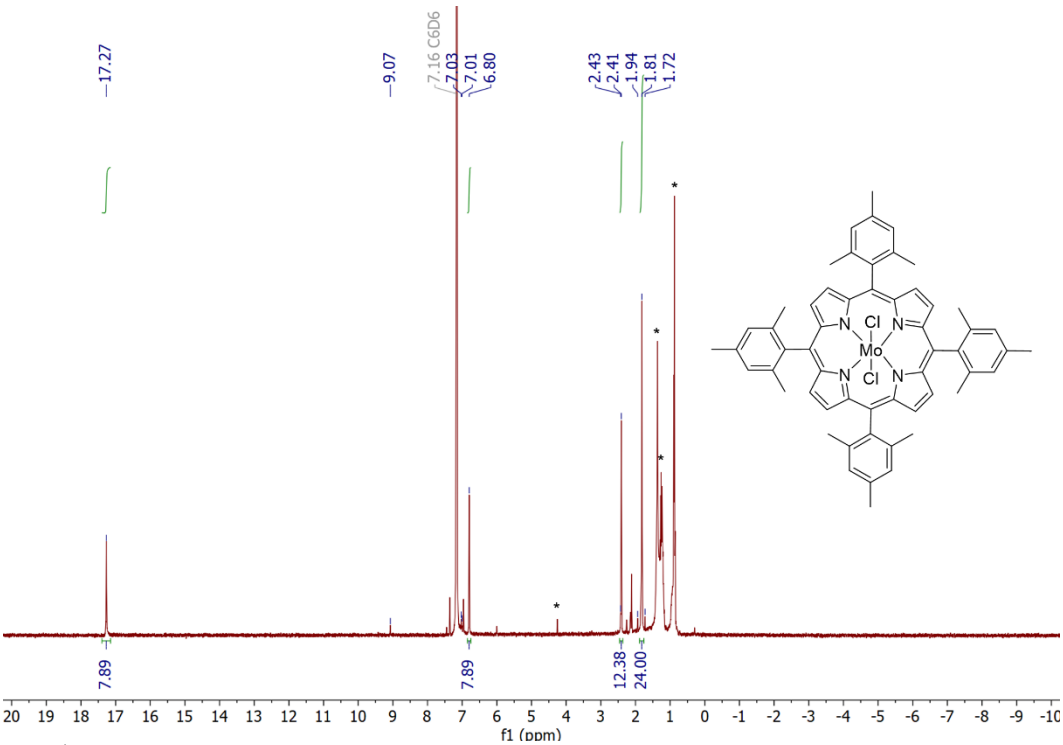

Figure S3: ^{1}H NMR spectrum of **2** in C_6D_6. Pentane, dichloromethane, and grease impurities are marked with *. Labeled peaks in the baseline are residual **1**.

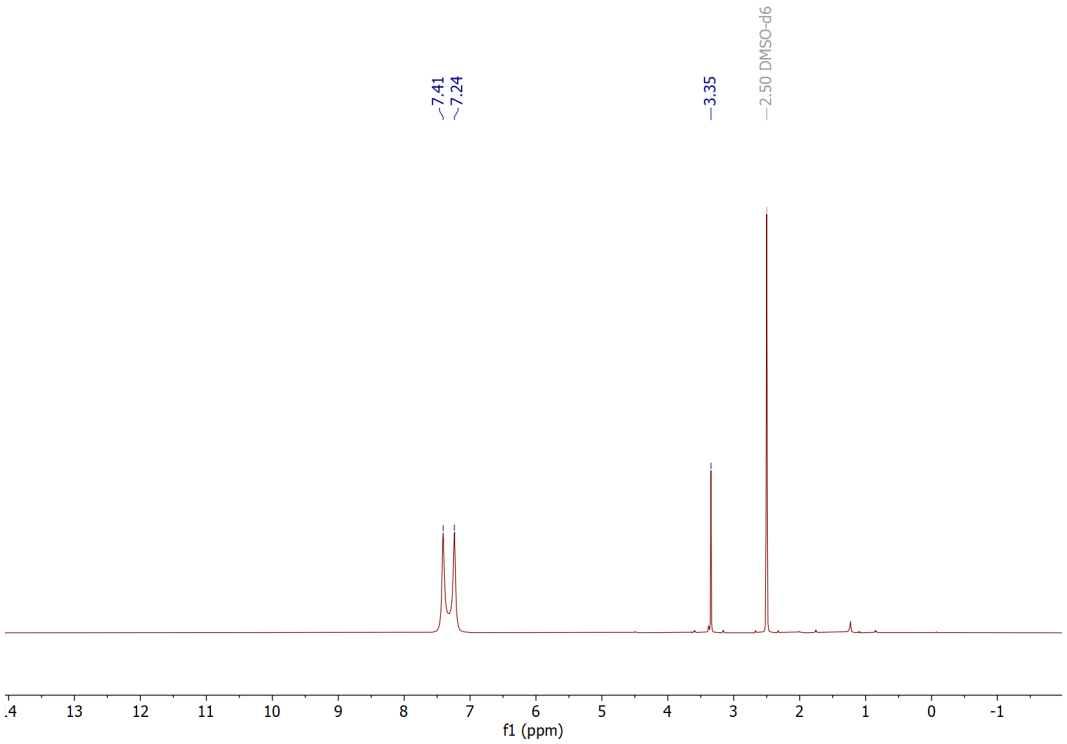

Figure S4: Qualitative ^{1}H NMR spectrum of the ammonium synthesized from a catalytic run of (TMP)MoN with $SmI_2(THF)_2$ and $(CH_2OH)_2$ under an atmosphere of $^{15}N_2$. After catalysis, the reaction mixture was basified, and volatiles were vacuum transferred onto HCl etherate before solvent was removed. The residue was taken up in DMSO-d_6. A water peak is present at 3.35 ppm.

IR Spectra

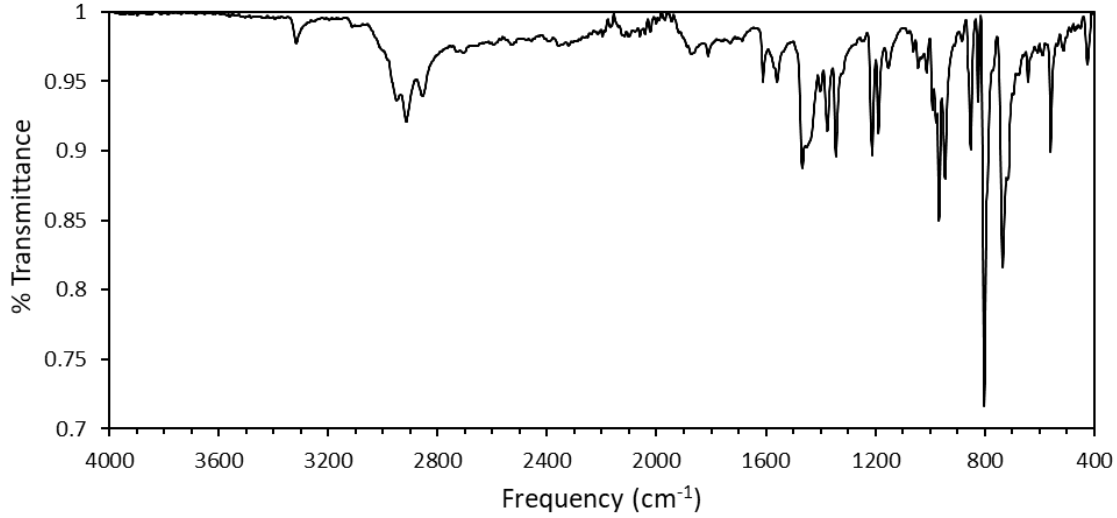

Figure S5: FT-IR spectrum of solid $TMPH_2$.

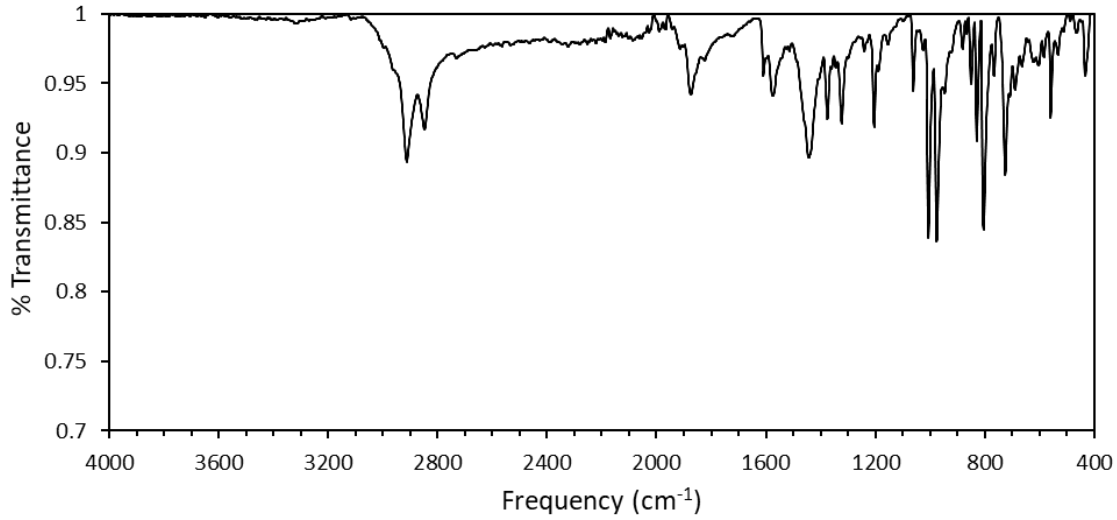

Figure S6: FT-IR spectrum of solid **1**.

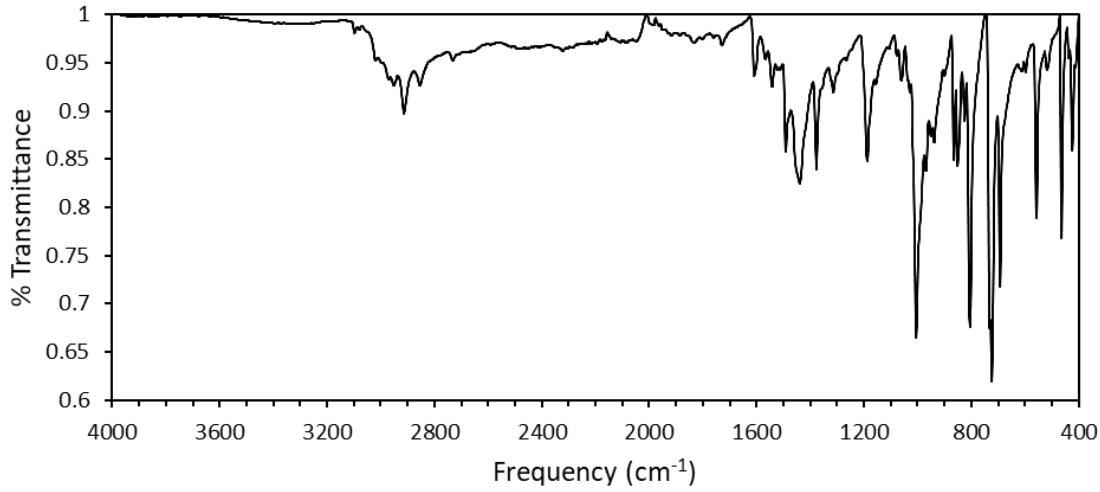

Figure S7: FT-IR spectrum of solid **2**.

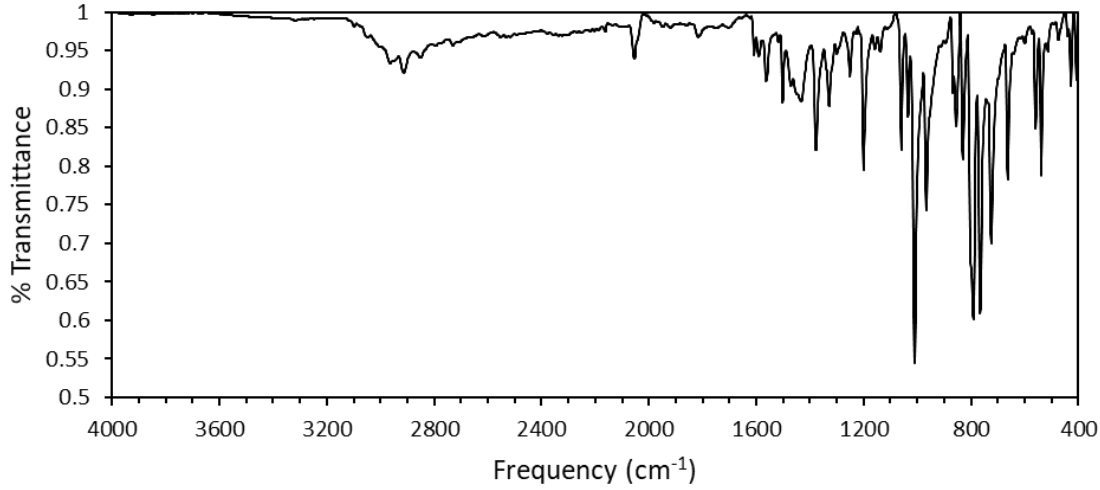

Figure S8: FT-IR spectrum of solid **3**.

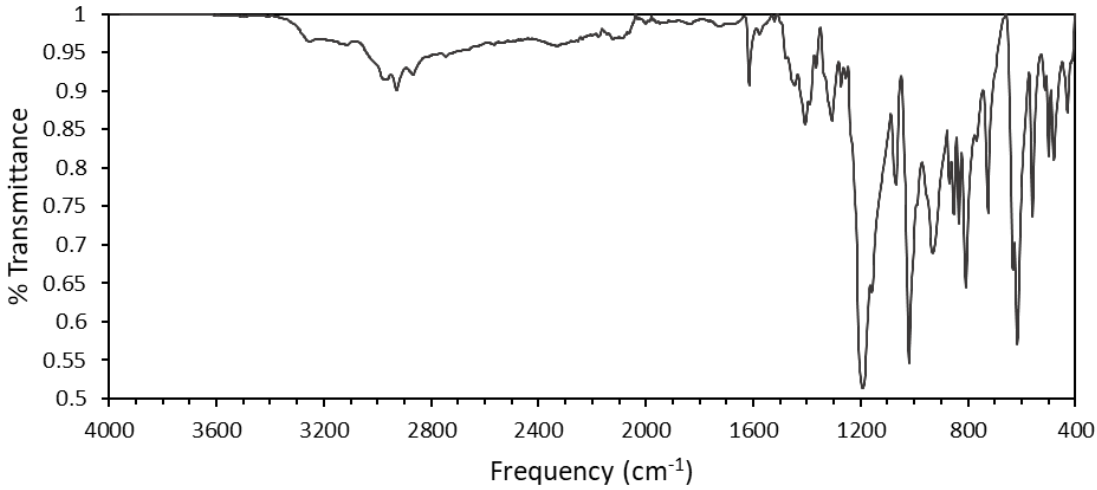

Figure S9: FT-IR spectrum of solid residue from reaction of **3** with TfOH in toluene.

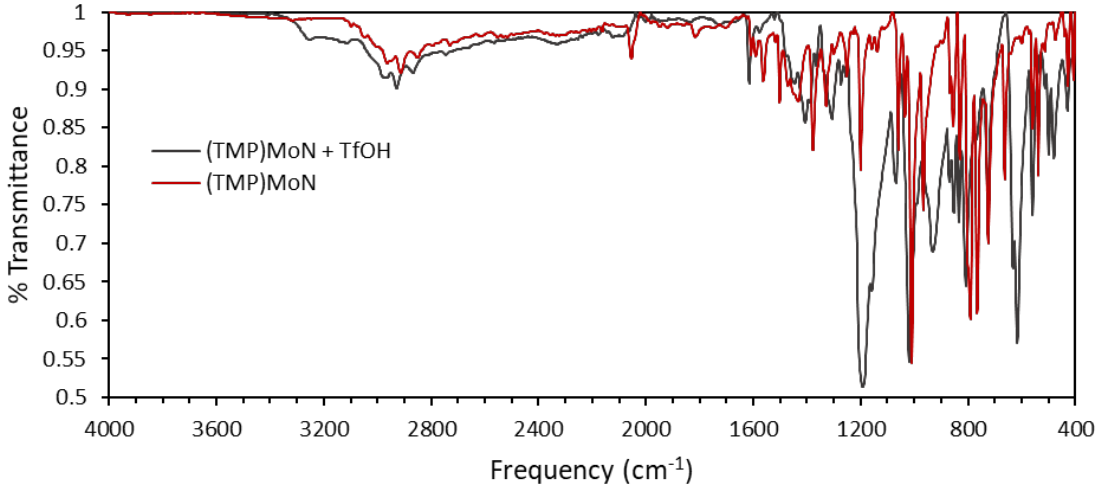

Figure S10: Overlay of the FT-IR spectra of **3** and the solid residue from reaction of **3** with TfOH in toluene.

UV-Visible Absorption Spectra

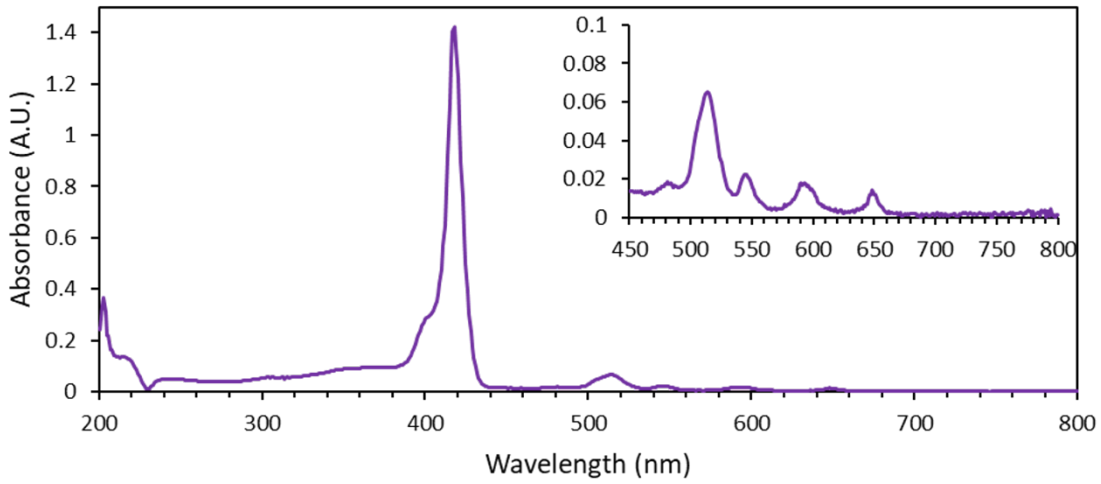

Figure S11: UV-visible spectrum of $TMPH_2$ in THF.

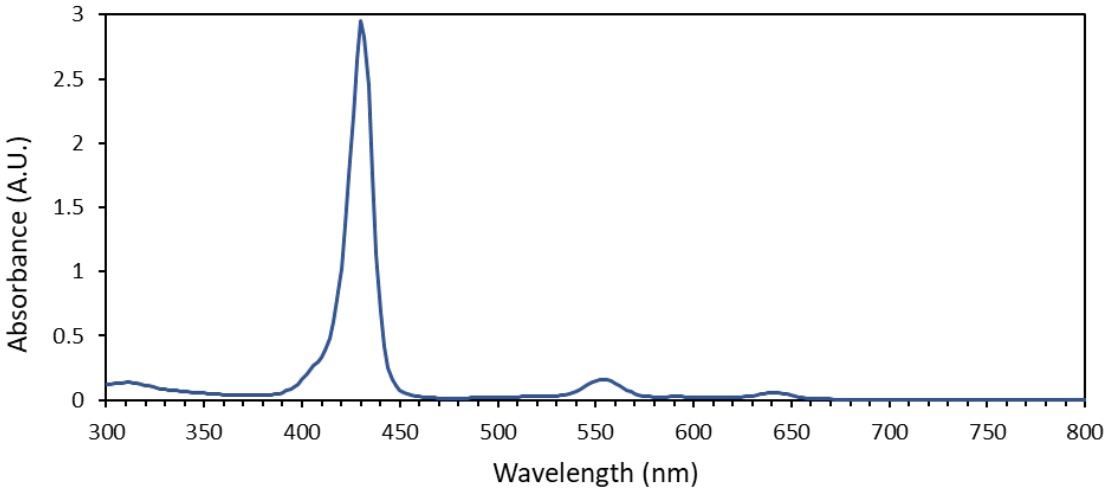

Figure S12: UV-visible spectrum of **1** in CH_2Cl_2.

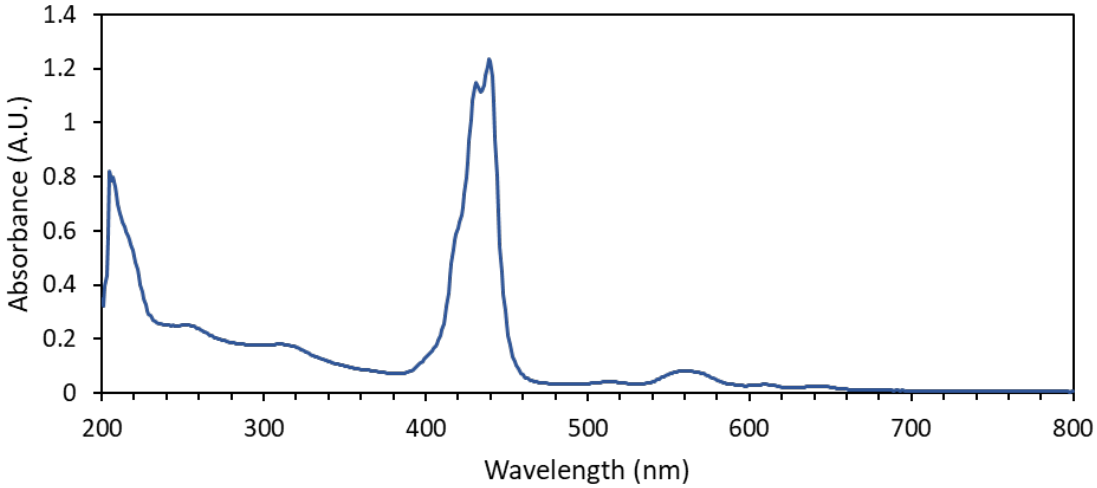

Figure S13: UV-visible spectrum of **1** in THF.

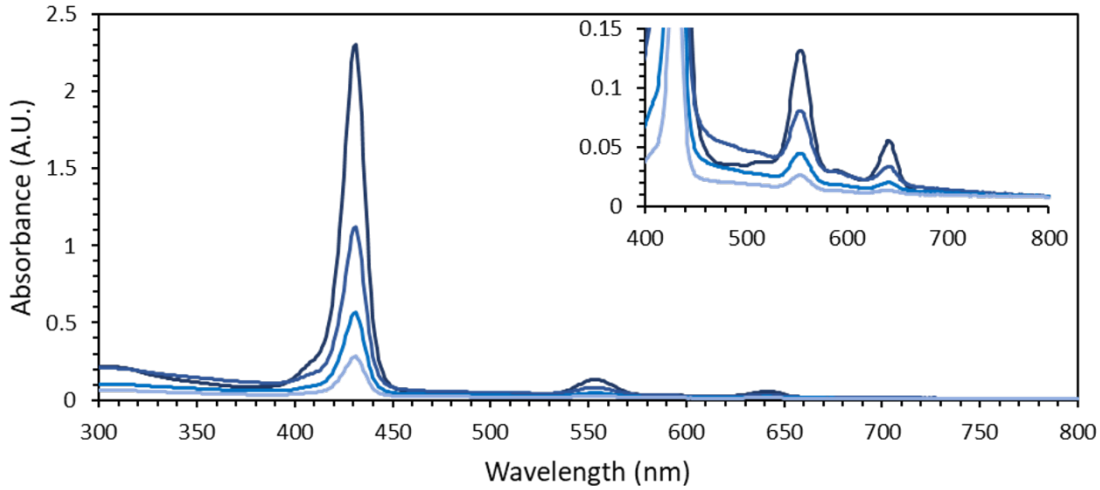

Figure S14: UV-visible spectrum of **1** in CH_2Cl_2 at various concentrations.

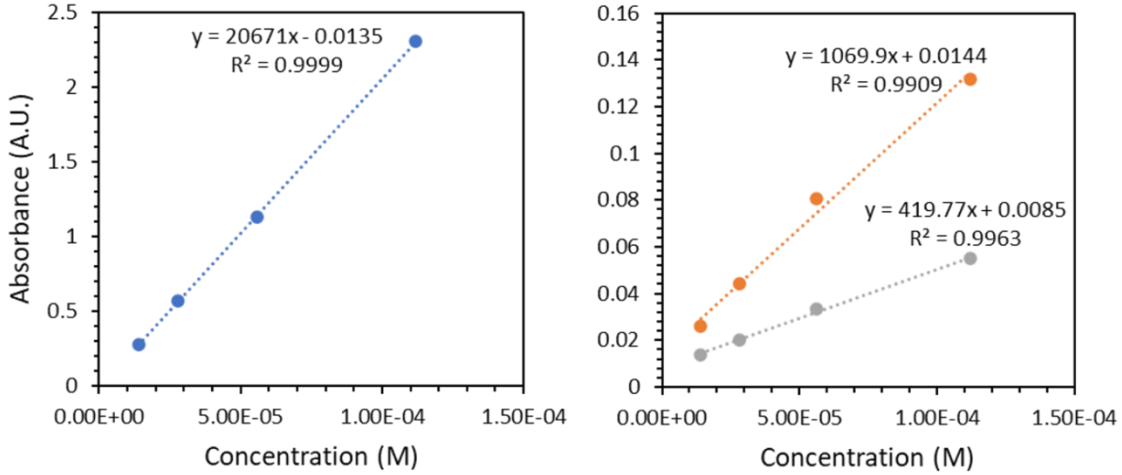

Figure S15: Beer-Lambert Law curve for **1** in CH_2Cl_2. The Soret band at 431 nm (ε = 210,000 cm^{-1} M^{-1}) is shown on the left in blue, and the β-band at 554 nm (ε = 11,000 cm^{-1} M^{-1}) on the right in orange with the α-band at 641 nm (ε = 4,200 cm^{-1} M^{-1}) in grey.

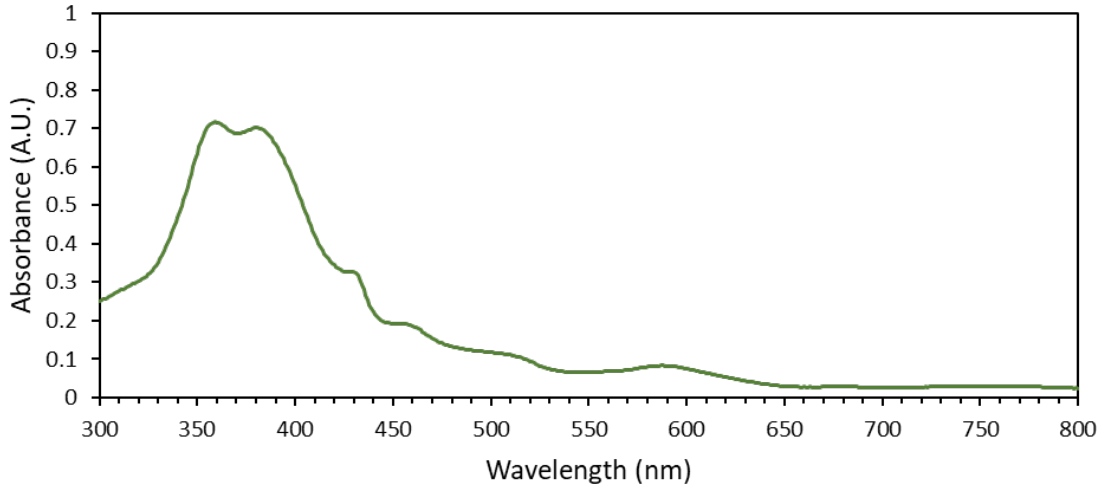

Figure S16: UV-visible spectrum of **2** in toluene.

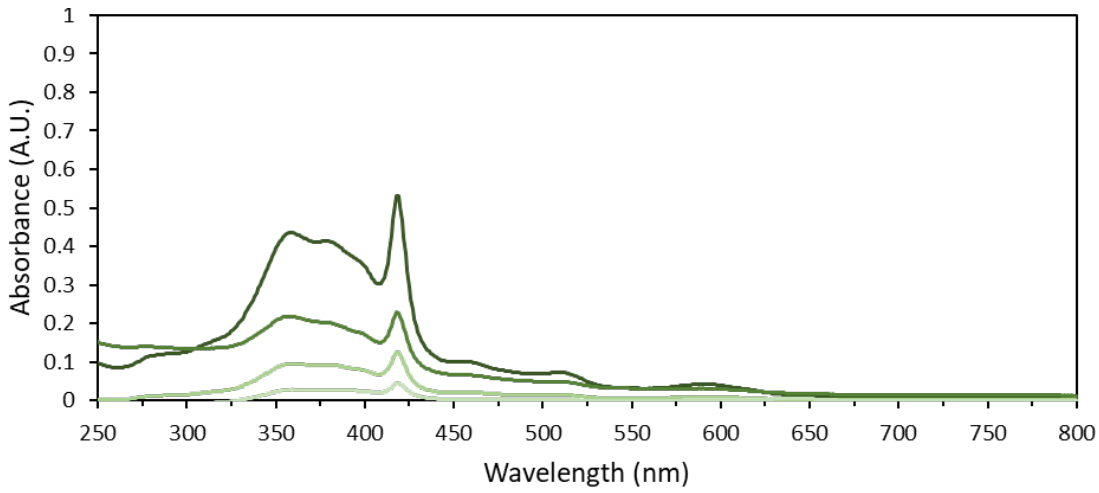

Figure S17: UV-visible spectrum of **2** in CH_2Cl_2 at various concentrations. Absorbance at 418 nm comes from residual $TMPH_2$, which was present in 0.00001% by mass and was not removed.

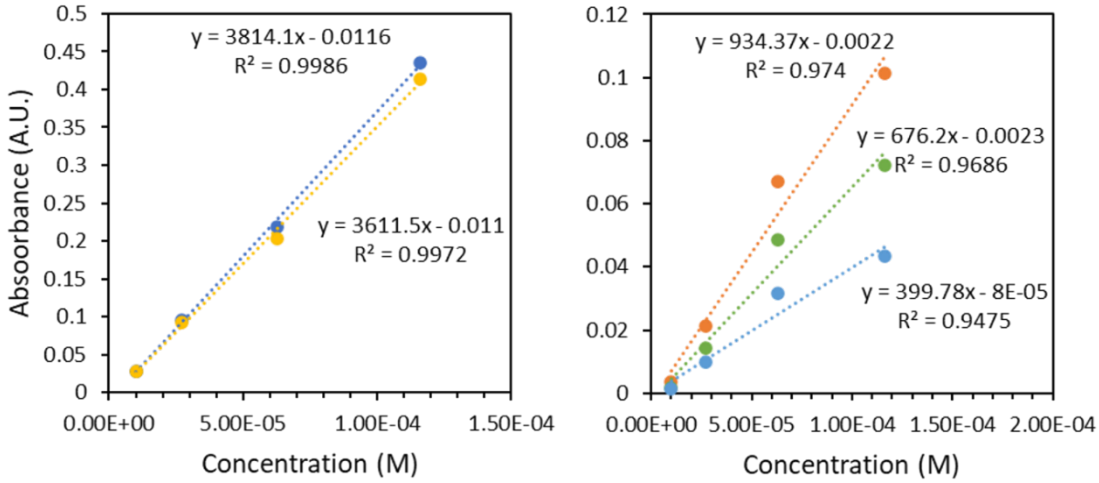

Figure S18: Beer-Lambert Law curve for **2** in CH_2Cl_2. The λ_{max} at 359 nm (ε = 38,000 cm^{-1} M^{-1}) in blue and the 378 nm band (36,000) in yellow are on the left. On the right the bands at 456 nm (9,300), 513 nm (6,800) and 592 nm (4,000) are shown in orange, green and blue, respectively.

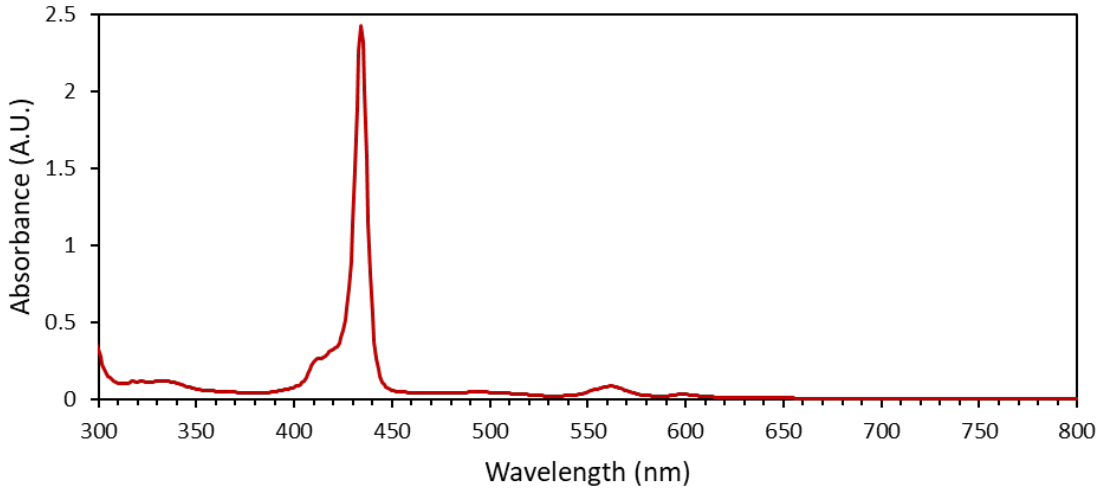

Figure S19: UV-visible spectrum of **3** in toluene.

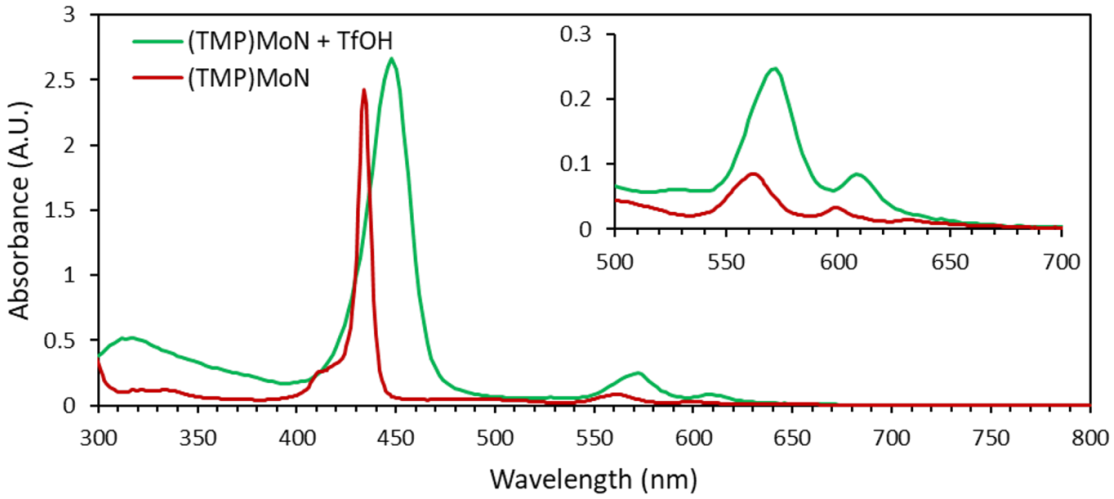

Figure S20: UV-visible spectrum of the reaction of **3** with triflic acid in toluene.

EPR Spectroscopy

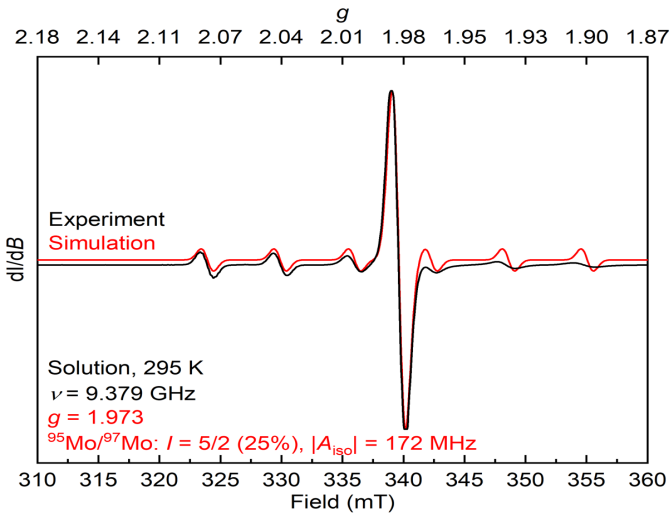

$$|A_{iso}| = 62.3\ G$$

Figure S21. X-Band EPR spectrum of **3** at 295 K (1.2 mM in toluene) measured with a microwave frequency of 9.379 GHz and power of 0.2019 mW. Parameters for simulation are listed in the figure in red. This matches the literature spectrum in ref. 2.

Electrochemistry Data

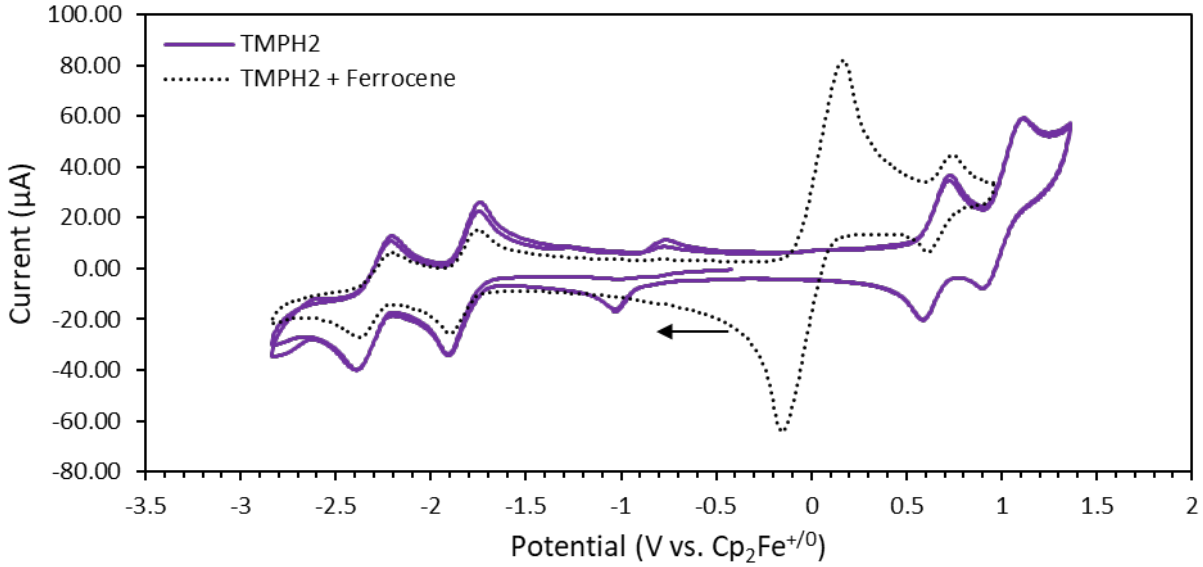

Figure S22: Cyclic voltammogram of $TMPH_2$ with and without ferrocene at a scan rate of 500 mV/s. OCP = −0.42 V vs $Fc^{+/0}$. The feature at −0.9 V vs $Fc^{+/0}$ is a result of oxidation products and is not observed when the window is set to avoid the second porphyrin oxidation.

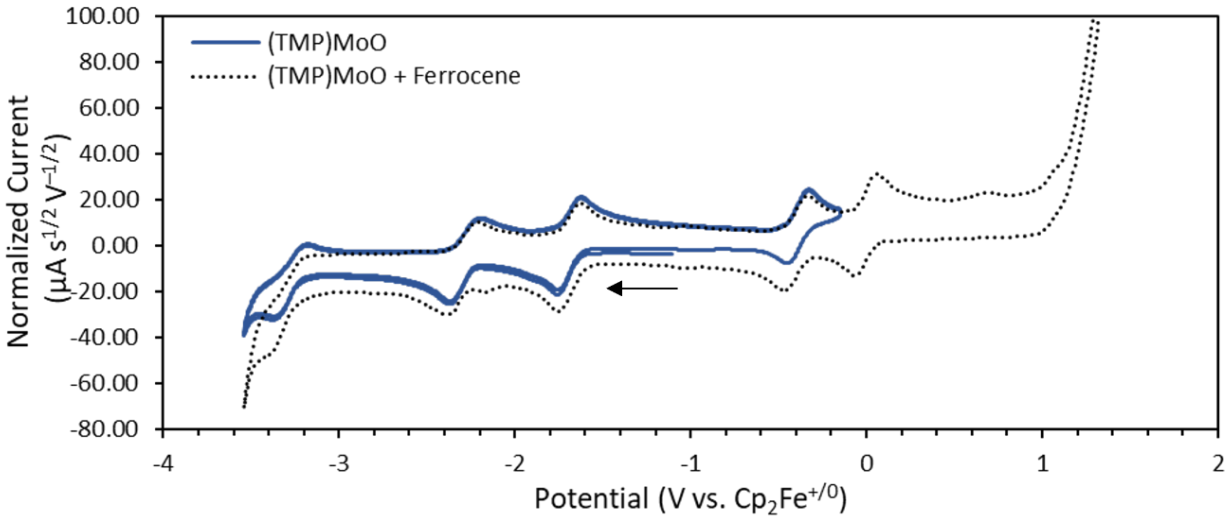

Figure S23: Cyclic voltammogram of **1** with and without ferrocene at a scan rate of 500 mV/s. OCP = −1.1 V vs $Fc^{+/0}$.

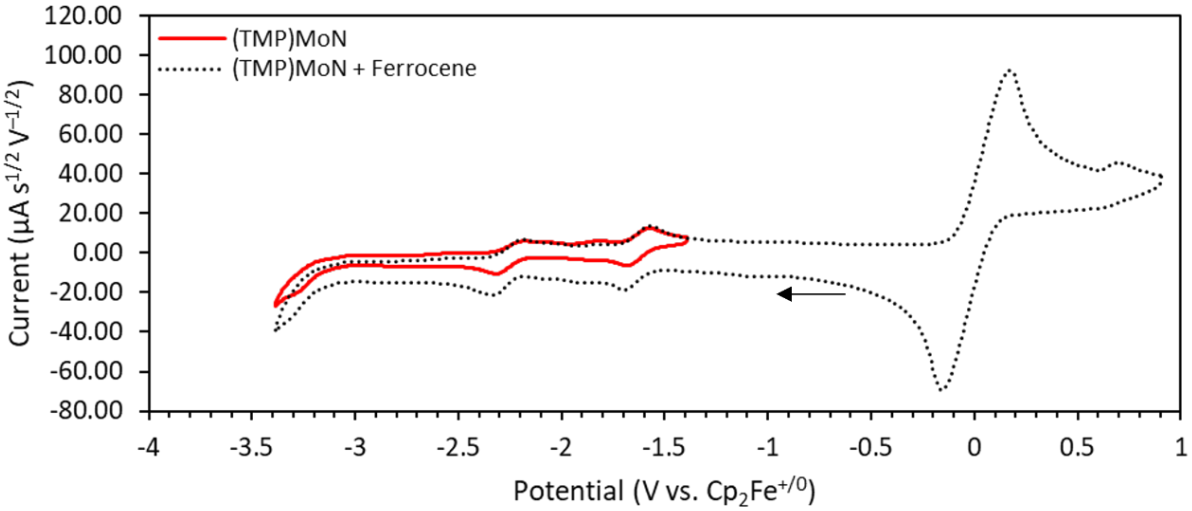

Figure S24: Cyclic voltammogram of **3** with and without ferrocene at a scan rate of 500 mV/s. OCP = −0.29 V vs $Fc^{+/0}$.

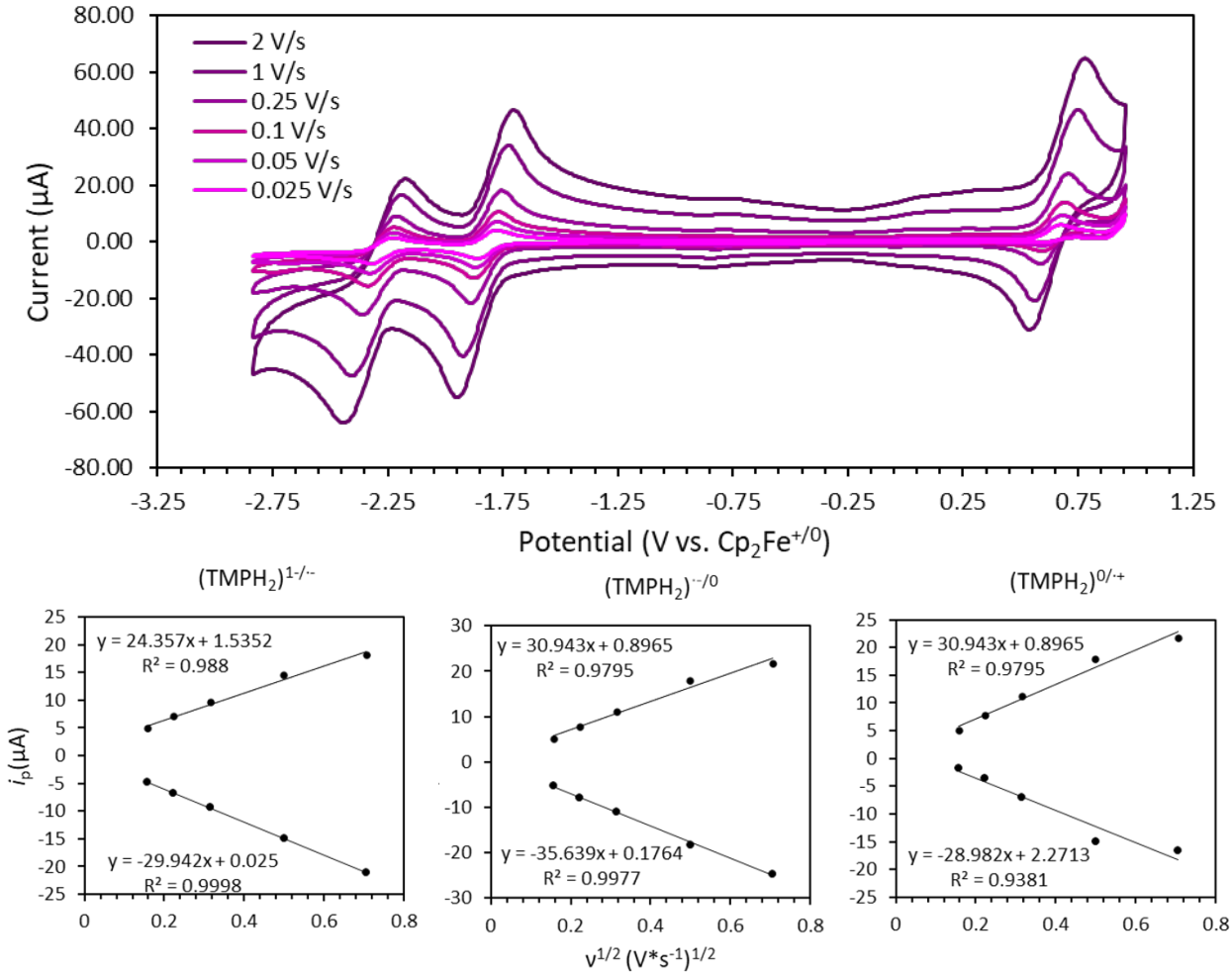

Figure S25: Scan rate dependence for $TMPH_2$ showing linear relationship between $v^{1/2}$ and peak current. Diffusion coefficient for $TMPH_2$ was calculated at $7.4 \cdot 10^{-7}$ cm^2/s from the average of the slopes for the $TMPH_2^{\cdot-/0}$ couple.

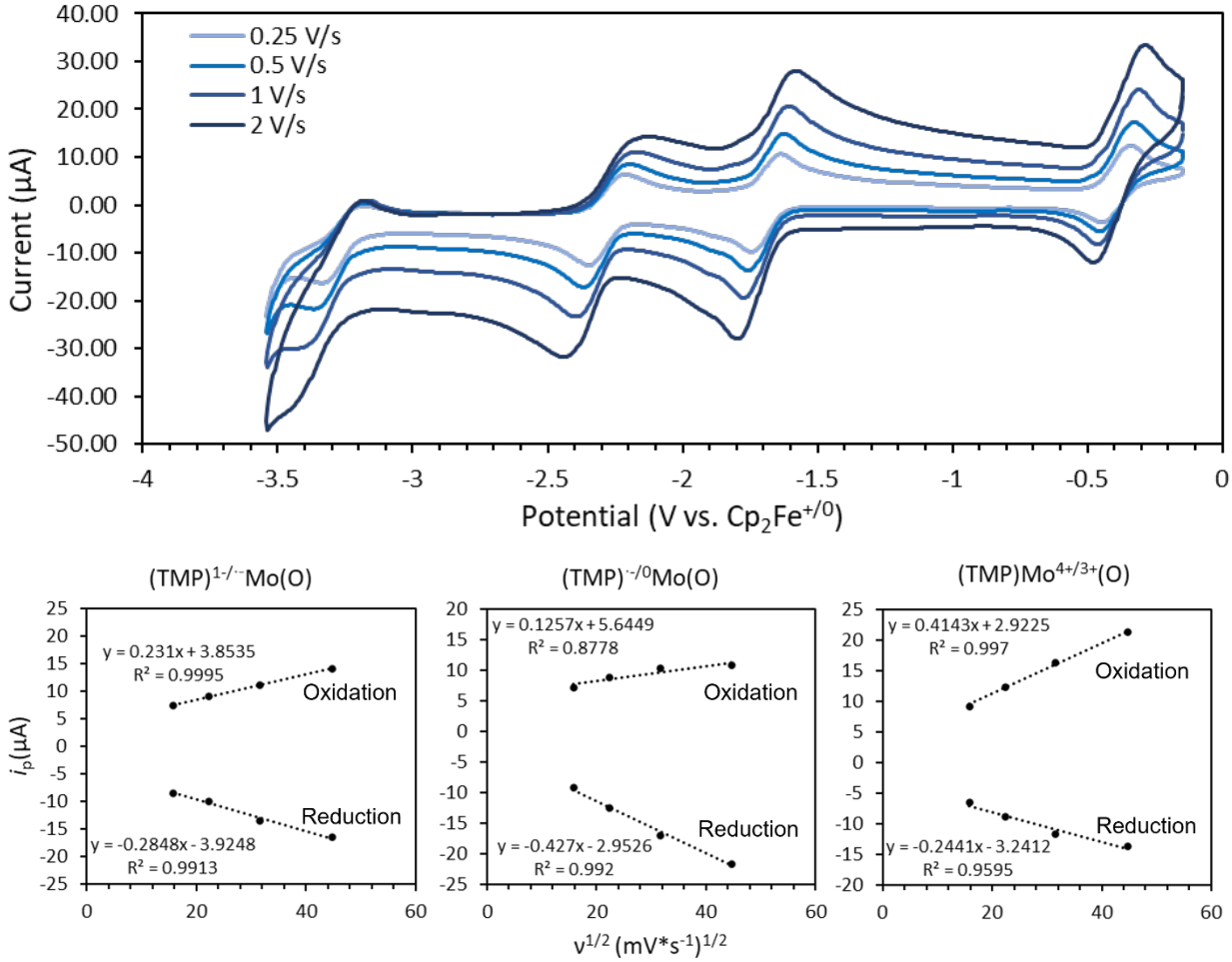

Figure S26: Scan rate dependence for **1** showing linear relationship between $v^{1/2}$ and peak current. Diffusion coefficients for (TMP)MoO were calculated for each oxidation state using the E_{pc} slopes. The first reduction $(TMP)^{\cdot-/0}Mo(O)$ had a diffusion coefficient $D_0 = 1.8 \cdot 10^{-7}$ cm^2/s, the second, $(TMP)^{1-/\cdot-}Mo(O)$, had $D_0 = 8.2 \cdot 10^{-8}$ cm^2/s, and the last reduction at molybdenum, the $(TMP)^{-}Mo^{4+/3+}(O)$ couple, the coefficient $D_0 = 6.0 \cdot 10^{-8}$ cm^2/s. The E_{pa} slopes were not averaged with the E_{pc} because each wave was not individually examined.

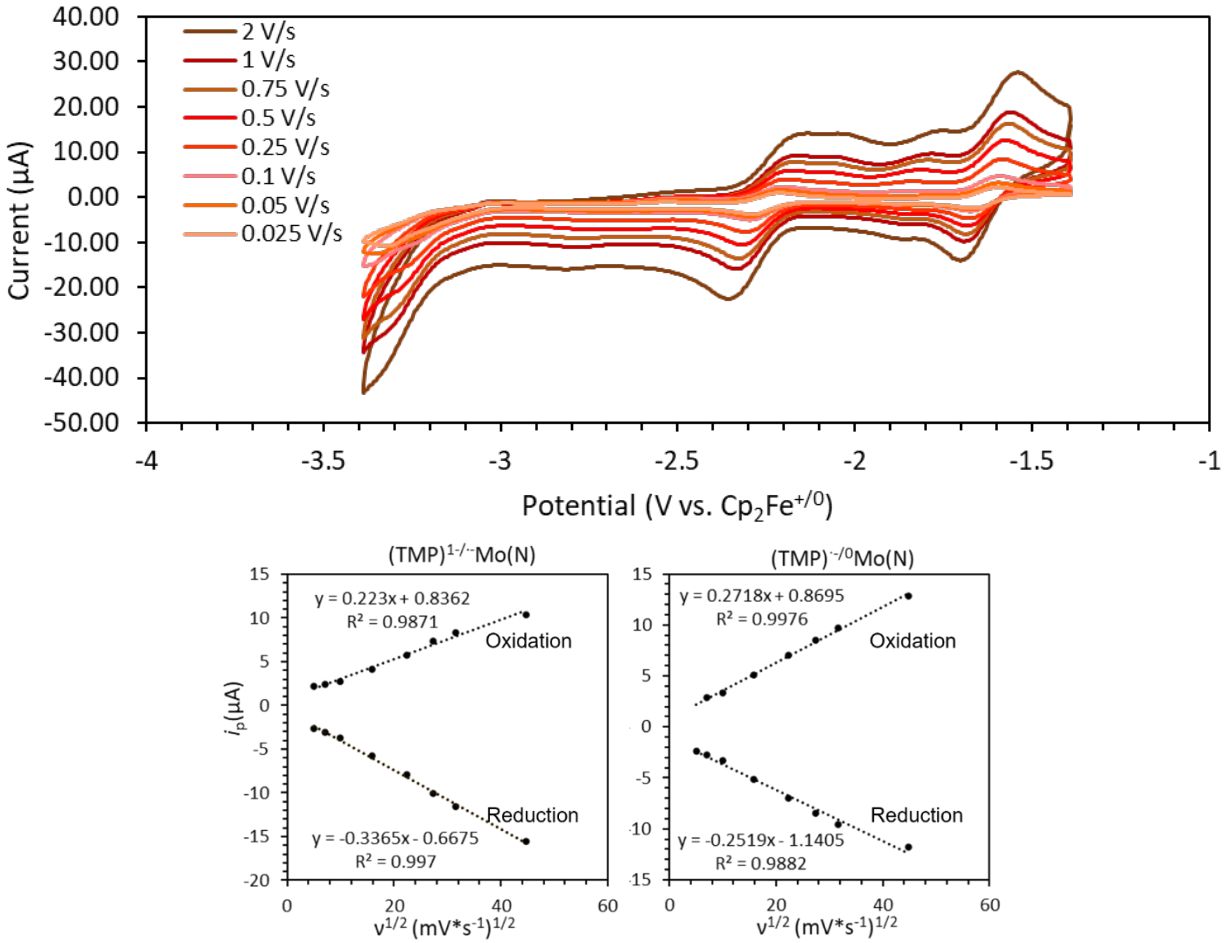

Figure S27: Scan rate dependence for **3** showing linear relationship between $v^{1/2}$ and peak current in TMP-based reductions. Diffusion coefficients for (TMP)MoN were calculated for each oxidation state using the average of the slopes for each couple. The first reduction $(TMP)^{\cdot-/0}MoN$ had a diffusion coefficient $D_0 = 1.3 \cdot 10^{-7}$ cm^2/s, the second, $(TMP)^{1-/\cdot-}MoN$, had $D_0 = 1.1 \cdot 10^{-7}$ cm^2/s.

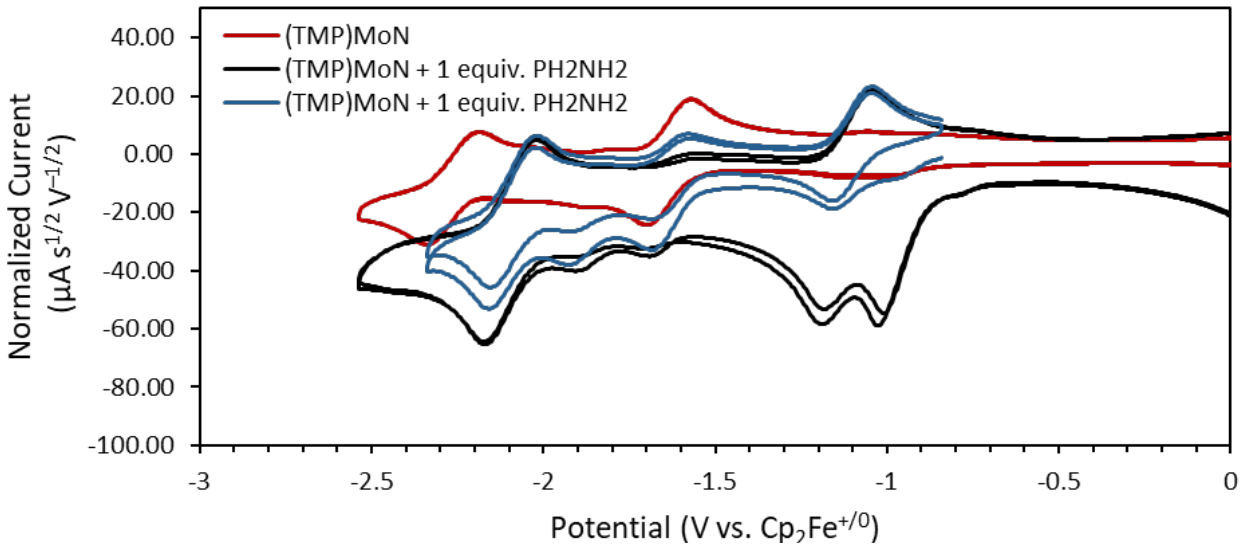

Figure S28: CVs of **3** with 1 equiv. $[Ph_2NH_2][OTf]$ at a scan rate of 500 mV/s. OCP = 0.34 V vs $Fc^{+/0}$.

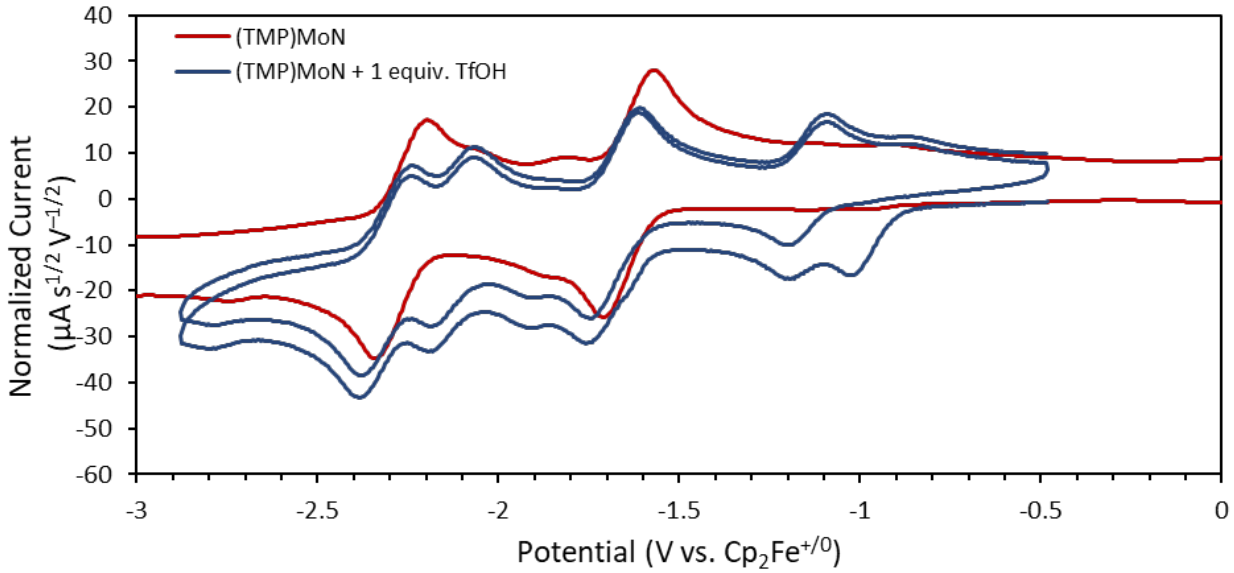

Figure S29: Cyclic voltammogram of **3** with and without 1 equiv. triflic acid at a scan rate of 500 mV/s. OCP = 0.25 V vs $Fc^{+/0}$.

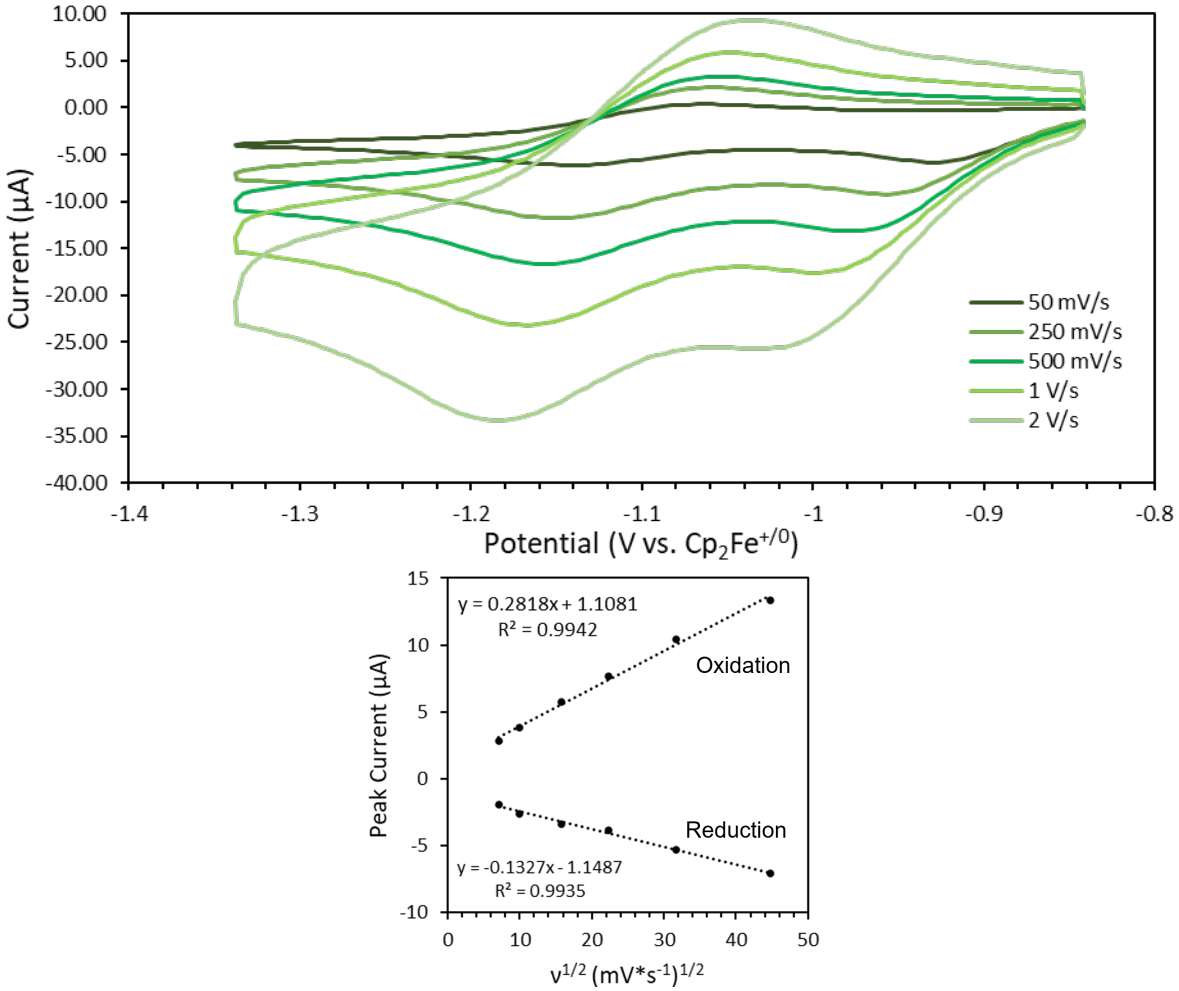

Figure S30: Scan rate dependence for **3** with 1 equiv. $[Ph_2NH_2][OTf]$ showing linear relationship between $v^{1/2}$ and peak current in the TMP-based reduction at −1.15 V vs $Fc^{+/0}$. The diffusion coefficient for $[(TMP)MoN]H^+$ was calculated using the average of the slopes at $D_0 = 2.5 \cdot 10^{-7}$ cm^2/s.

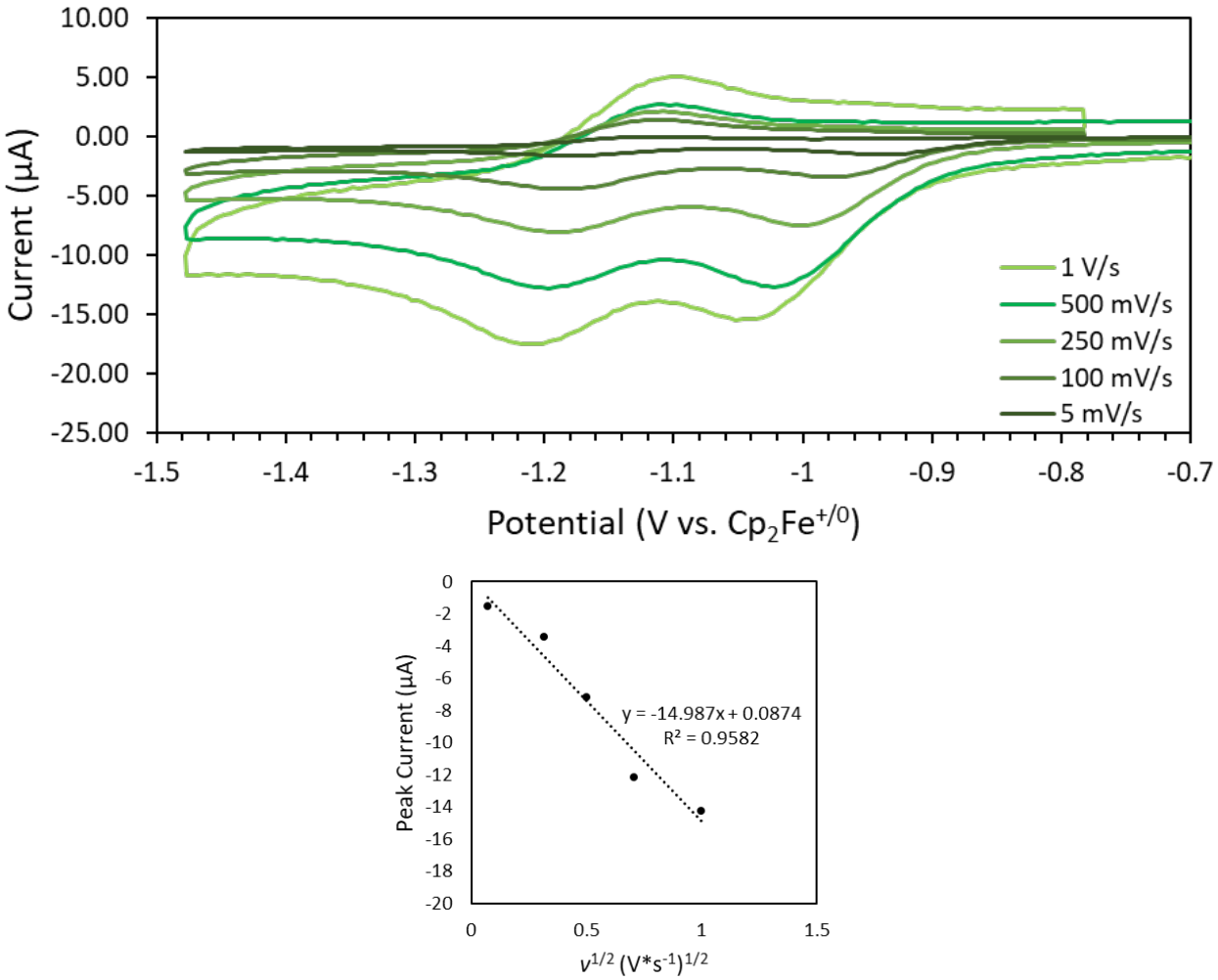

Figure S31: Scan rate dependence for **3** with 1 equiv. HOTf showing linear relationship between $v^{1/2}$ and peak current for the E_{pc} of the irreversible reduction at −0.945 V vs $Fc^{+/0}$. Since the diffusion coefficients were similar for all of the (TMP)Mo complexes, we made the assumption that the constant for the protonated species in solution would be similar as well. Using the average diffusion coefficient for the E_{pc}'s of $[(TMP)MoN]H^+$, (TMP)MoO and (TMP)MoN, the number of electrons passed in the irreversible wave was calculated at n = 1.1 electrons = 1 electron.

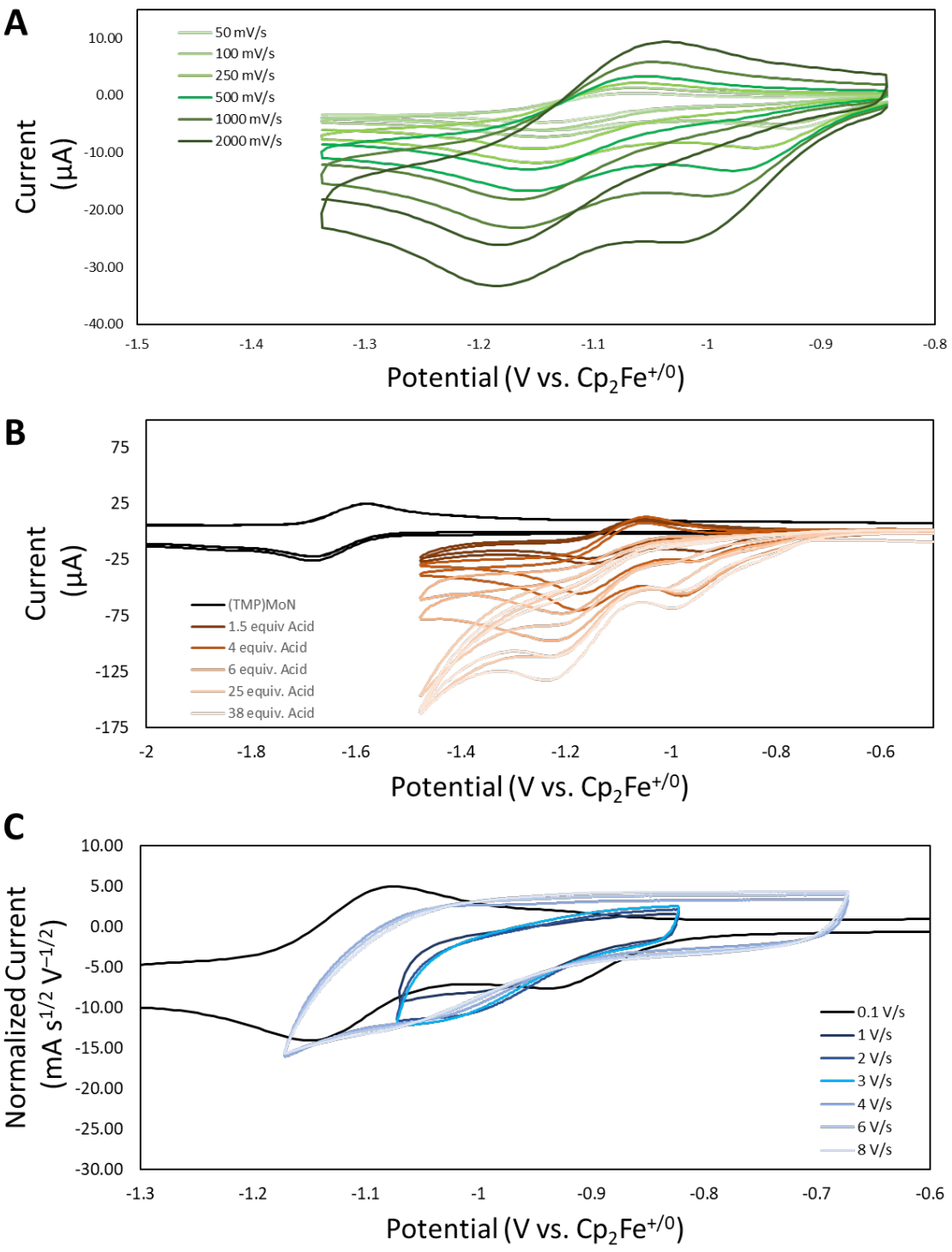

Figure S32: CVs of (TMP)MoN following protonation with $[Ph_2NH_2][OTf]$. **A)** Variable scan rate of the first two reductions. **B)** Variable acid concentration. **C)** Elevated scan rate of the first reduction to check for reversibility.

Spectroelectrochemistry

In a UV-SEC experiment, electrochemical reduction of the species of interest was monitored by UV-Vis spectroscopy in an OTTLE cell. Conditions: THF, 0.2 M [^{n}Bu$_4$N][PF$_6$], N_2 atmosphere, OTTLE cell (gold wire mesh working electrode, Pt wire mesh counter electrode, Ag reference electrode). First, the potential of the cell was swept negatively recording a thin-layer cyclic voltammogram or a linear sweep voltammogram (5 mV/s) to identify the potential window of interest. Then, fresh analyte solution was introduced in the cell and an initial spectrum was obtained. Controlled potential bulk electrolysis (CPE) experiments were run while recording a UV-visible spectrum every 15 seconds until no further changes were observed to the spectrum. The potential was either set to 100 mV negative of the reduction potential of interest and held there for the duration of the experiment, or set to 300 mV positive of the reduction potential of interest and stepped cathodically by 100 mV after a minute of CPE and recording spectral changes.

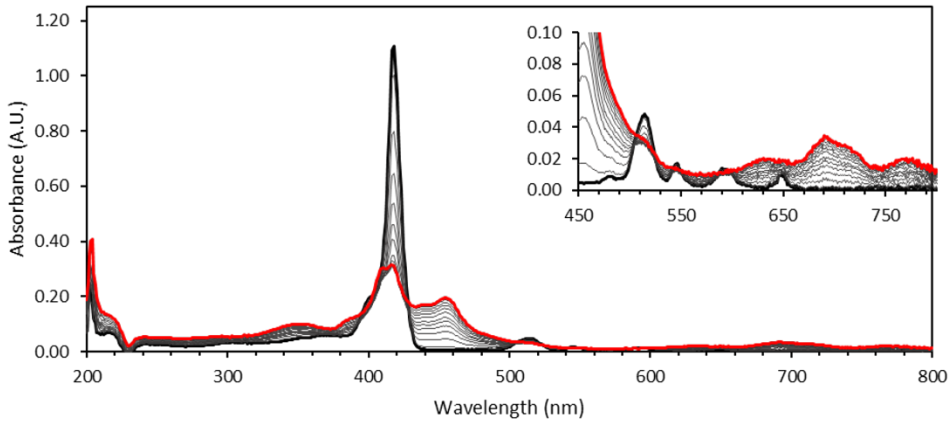

Figure S33: UV-SEC plot of the reduction of 0.25 mM $TMPH_2$ at −1.8 V vs Fc^+/Fc. Initial scan = black, final scan = red. Inset shows the 500-800 nm range for the same reduction.

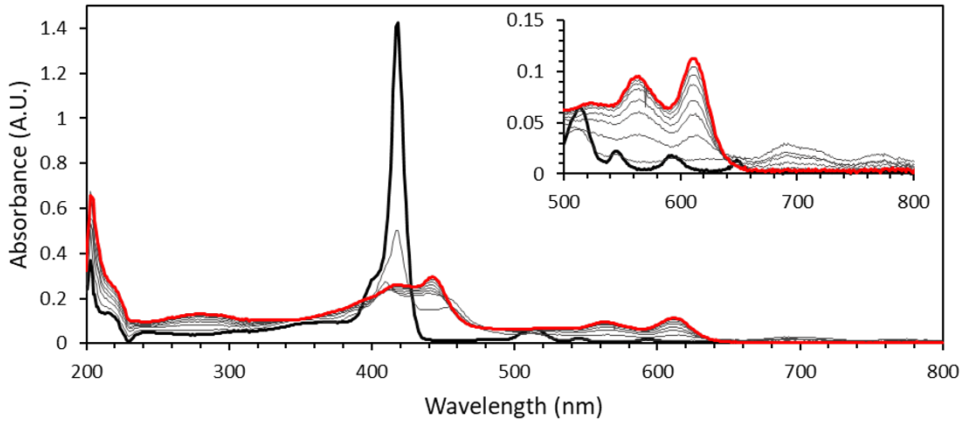

Figure S34: UV-SEC plot of the reduction of 0.25 mM $TMPH_2$ at −2.5 V vs Fc^+/Fc. Initial scan = black, final scan = red. Inset shows the 500-800 nm range for the same reduction. Features around 650-800 nm appear as the first reduction occurs, then disappear during the second reduction.

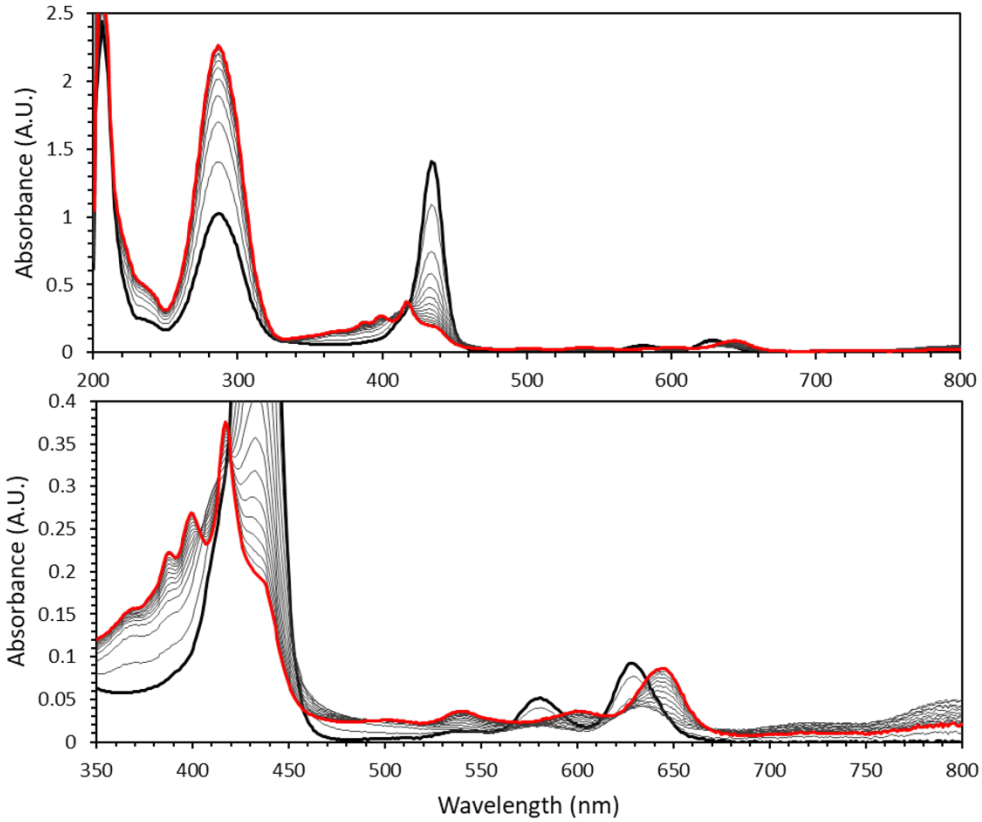

Figure S35: UV-SEC plot of the reduction of 0.25 mM $TMPH_2$ in the presence of 20 equivalents $[Ph_2NH_2]OTf$ at −1.0 V vs Fc^+/Fc. Initial scan = black, final scan = red. Top spectrum shows the full window, and the bottom spectrum focuses in on the smaller features in the 350-800 nm range for the same reduction. The large absorbance at 286 nm is from the acid. Unlike the previous UV-SEC experiments for $TMPH_2$, this change was irreversible upon returning the potential.

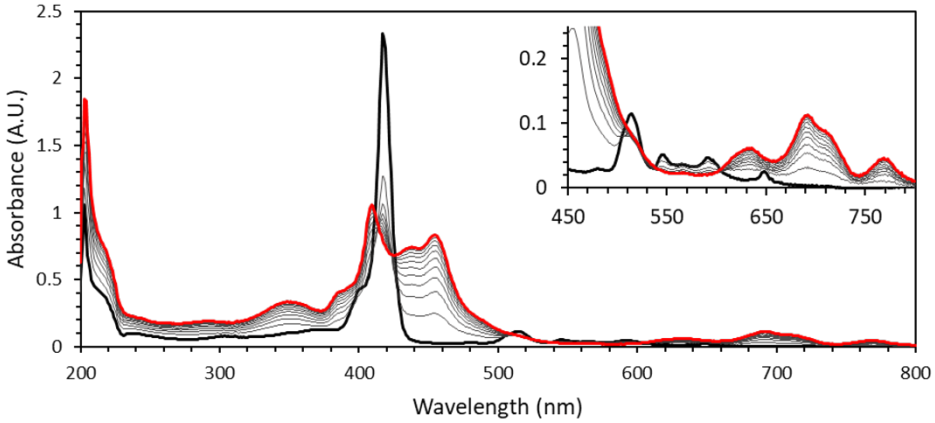

Figure S36: UV-SEC plot of the reduction of 2.7 mM $TMPH_2$ in the presence of 2.6 equiv. $[HNEt_3]PF_6$ at −2 V vs Fc^+/Fc. Initial scan = black, final scan = red. Inset shows the 450-800 nm range for the same reduction. Surprisingly, this change was reversible upon switching the potential of the electrode to −1 V vs Fc^+/Fc.

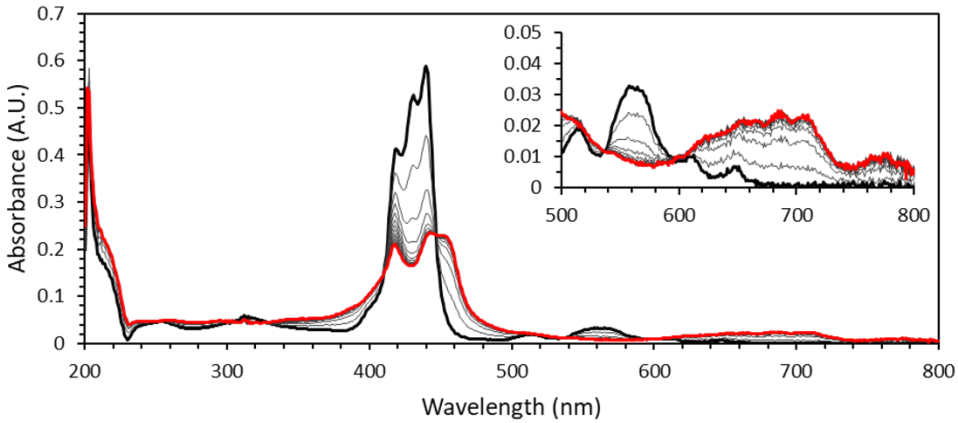

Figure S37: UV-SEC plot of the reduction of 0.15 mM **1** at −1.8 V vs Fc^+/Fc. Initial scan = black, final scan = red. Inset shows the 500-800 nm range for the same reduction.

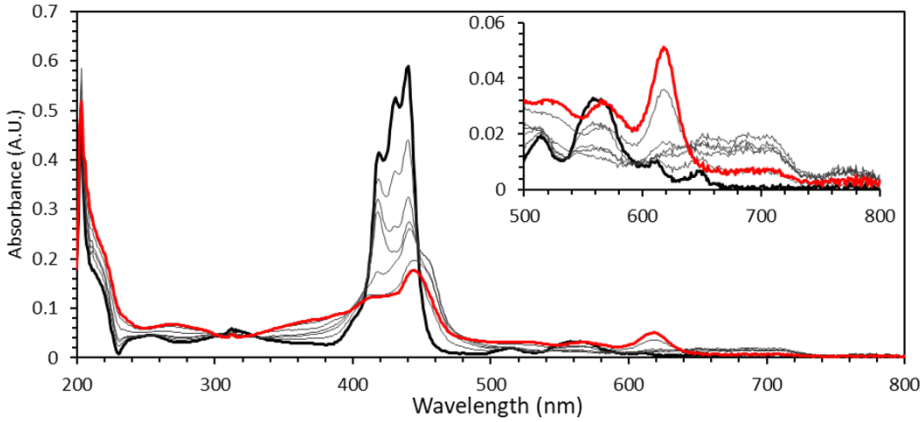

Figure S38: UV-SEC plot of the reduction of 0.15 mM **1** at −2.4 V vs Fc^+/Fc. Initial scan = black, final scan = red. Inset shows the 500-800 nm range for the same reduction.

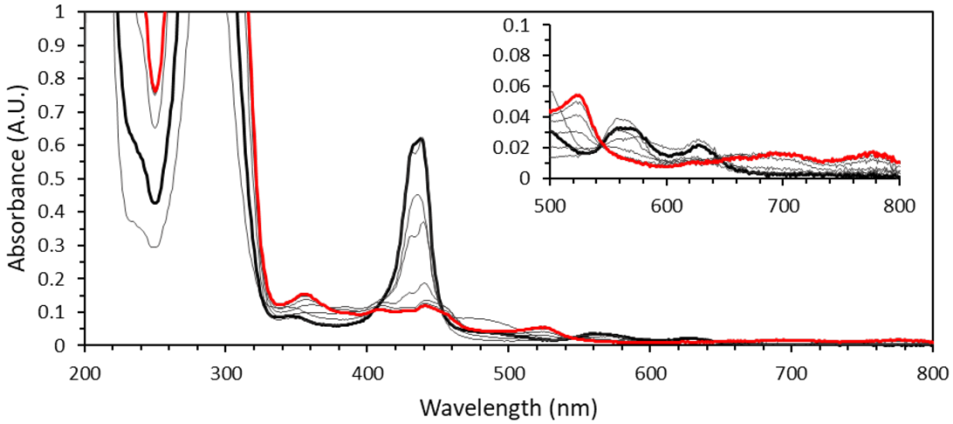

Figure S39: UV-SEC plot of the reduction of 0.15 mM **1** in the presence of 80 equivalents $[Ph_2NH_2]OTf$ at −2.5 V vs Fc^+/Fc. Initial scan = black, final scan = red. Inset shows the 500-800 nm range for the same reduction. The large absorbance at 286 nm is from the acid.

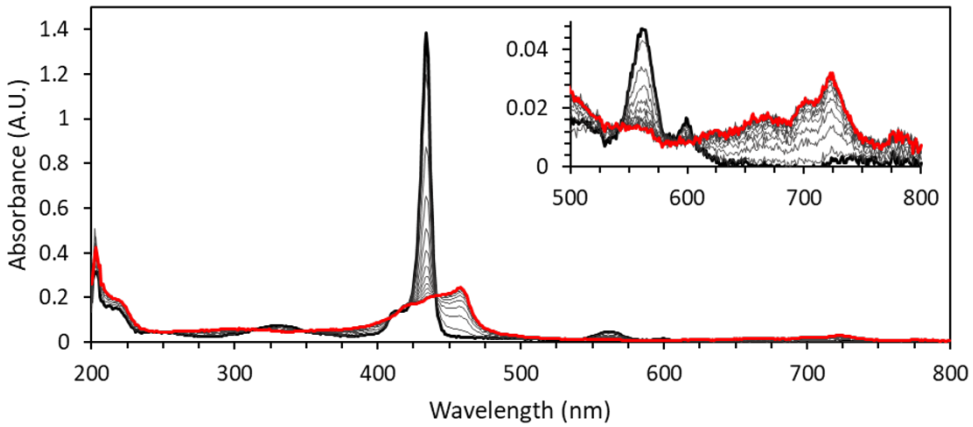

Figure S40: UV-SEC plot of the reduction of 0.2 mM **3** at −1.7 V vs Fc^+/Fc. Initial scan = black, final scan = red. Inset shows the 500-800 nm range for the same reduction.

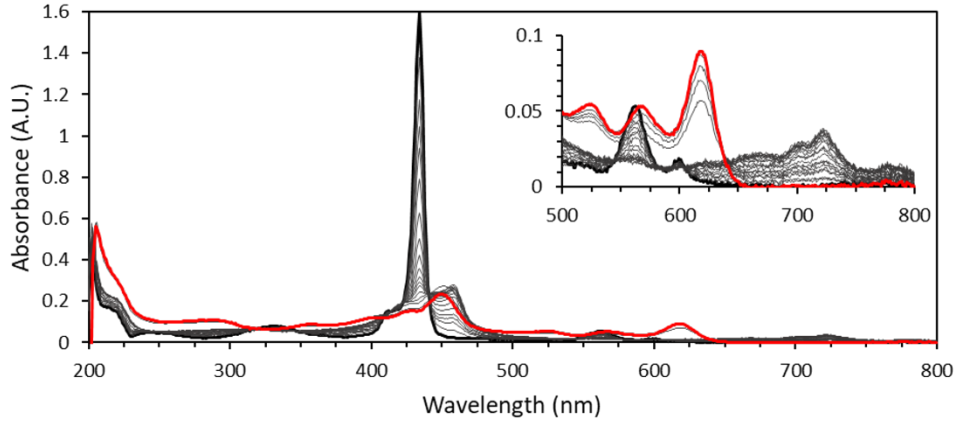

Figure S41: UV-SEC plot of the reduction of 0.2 mM **3** at −1.5 V vs Fc^+/Fc, before stepping the potential down to −2.3 V vs Fc^+/Fc. Initial scan = black, final scan = red. The dramatic change in the absorbance occurs within the first 30 seconds when the potential was switched to −2.3 V. Inset shows the 500-800 nm range for the same reduction.

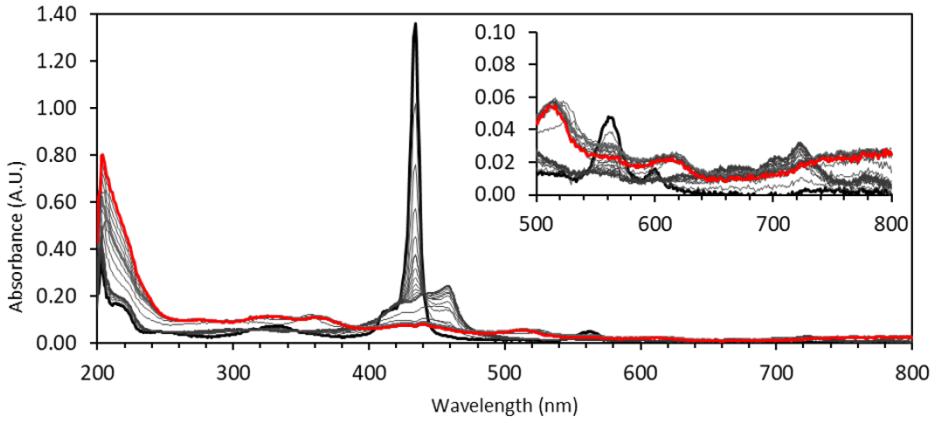

Figure S42: UV-SEC plot of the reduction of 0.2 mM **3** at −1.5 V vs Fc^+/Fc, before stepping the potential down to −3.1 V vs Fc^+/Fc. Initial scan = black, final scan = red. Inset shows the 500-800 nm range for the same reduction.

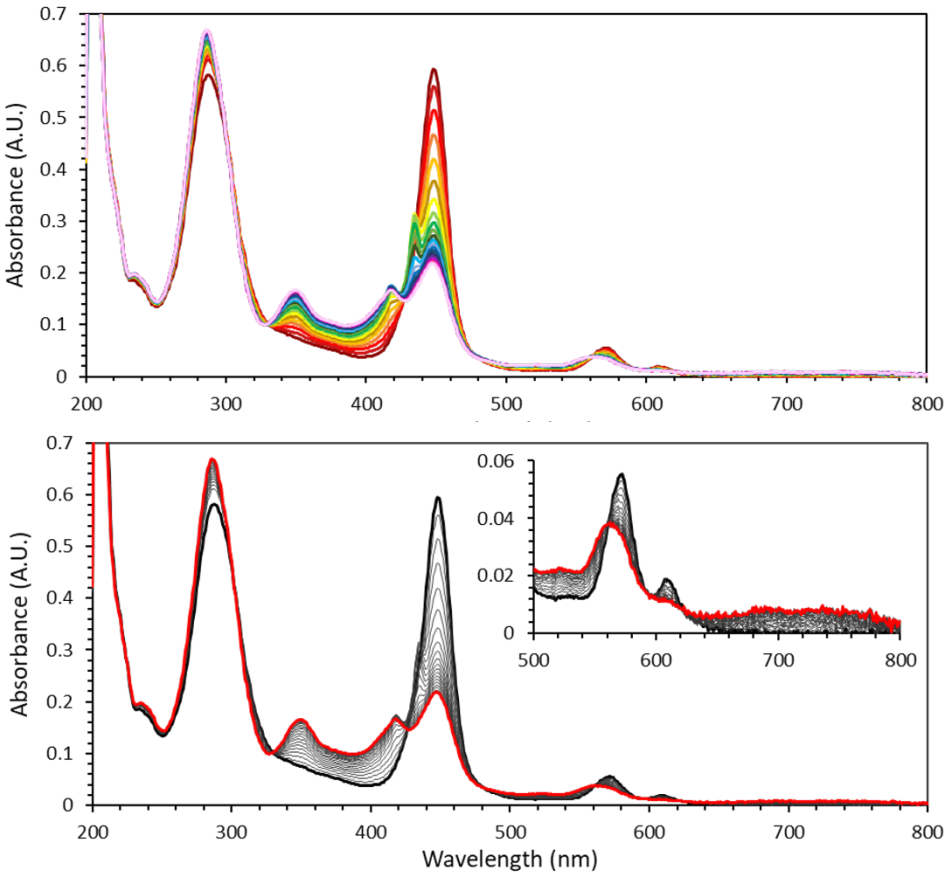

Figure S43: UV-SEC plot of the reduction of 0.2 mM **3** in the presence of 6 equivalents $[Ph_2NH_2]OTf$ at −1.0 V vs Fc^+/Fc. Top spectrum is in color to better view the reappearance and subsequent loss of the Soret band of **3** during electrolysis, and the bottom spectrum has the black to red progression of other UV-SEC plots. The large absorbance at 286 nm is from the acid. Bubbles were seen in the cell after reduction. The spectral changes were irreversible upon returning the potential.

Catalysis

NH_4^+ Isolation and Quantification Procedure

For reactions that require the separation of NH_4^+ from the metal-containing products the following procedure was followed using a specialty glass apparatus. This apparatus is comprised of two bomb-flasks fused together with a 3-way bridge which connects the two flasks and a ground-glass (GG) adapter. The bridge is gated with three Kontes valves, one at each bridge-flask and bridge-GG adapter junction.[5]

After the NH_4^+-generating reaction ceased, the sealed apparatus was removed from the glovebox and connected to a Schlenk line with the GG adapter. The product mixture was then frozen using liquid nitrogen. After the mixture was completely frozen the PTFE pin was removed from the flask and a MeOH solution (<10% of the volume of the reaction mixture) containing NaO^{t}Bu (2x total mol of acid in the reaction mixture) was added dropwise to the frozen mixture, taking care not to thaw the solution. After the addition the PTFE pin was replaced, and the flask was sealed and left in the liquid nitrogen for an additional 10 minutes. The second compartment of the apparatus was opened, and the PTFE pin was removed. HCl etherate (2M, 2x mol of NaO^{t}Bu added to the reaction mixture) was added, the PTFE pin was replaced, the flask was sealed, and the solution was also frozen with liquid nitrogen. Once the contents of both flasks were completely frozen, the headspaces of the bridge and flasks were evacuated with dynamic vacuum. Once the pressure stopped changing, all three Kontes valves were sealed to isolate the apparatus under static vacuum. The flask containing the reaction mixture was thawed and left to stir at room temperature for 10 minutes. After this time, the volatile components were condensed into the second flask via vacuum transfer while the HCl solution was kept frozen using liquid nitrogen. This step was preformed carefully as to avoid bumping. Once the vacuum transfer was complete the receiving flask was sealed, thawed, and stirred at room temperature for 10 minutes. After this time, the volatile components were removed with vacuum. The remaining solids were dissolved in high purity deionized water (10 mL) and filtered through a 0.45 μm syringe filter prior to analysis with ion chromatography (IC).

H_2 Quantification Procedure

Catalytic runs in which H_2 was quantified were run in a 25 mL round bottom flask with a well-greased linear vacuum adapter attached to maintain the headspace during the overnight reaction. The reaction was set up and run in a N_2 filled glovebox and the vacuum adapter was fitted with a rubber septum prior to removing for headspace analysis. Following a catalytic reaction, the solution was chilled for 10 min in a dry ice/isopropanol bath to remove THF vapor from the headspace. Methane gas (1.5 mL) was added via airtight syringe into the headspace of the reaction flask as an internal standard, the solution was stirred in the bath for 10 min, and then 150 μL of the headspace of the flask was removed via airtight syringe for H_2 quantification on the GC. H_2 present was determined via comparison to a calibration curve, shown below, of the observed peak area ratios versus the known ratio of gasses present.

It was not possible to fully separate the hydrogen and methane peaks, so the chromatogram was fit to two Gaussian curves in Microsoft Excel, and the individual curves were integrated to determine the observed ratio of CH_4 to H_2 responses. The raw data and fits are shown below in figure S46.

$$N_2 + 6\ SmI_2(THF)_2 + 6\ (CH_2OH)_2 \xrightarrow[THF,\ RT]{[Mo\ Catalyst]} 2\ NH_3 + 6\ SmI_2(OR)\ (+\ H_2)$$

Entry	Catalyst	Equiv. SmI_2/ROH	Equiv. NH_4^+ / Mo	% Yield NH_3[a]	Equiv. H_2 / Mo	% Yield H_2[a]
1	(TMP)MoO	180.2	25.6	42.6%	47.3	52.5%
2		179.7	24.7	41.3%	44.7	49.7%
3		179.1	25.5	42.6%	39.4	44%
4	(TMP)$MoCl_2$	186.5	16.0	25.8%	36.6	39.2%
5		179.8	18.0	30.0%	51.8	57.7%
6		186.3	11.5	18.5%	63.5	68.2%
7	(TMP)MoN	179.2	35.7	59.8%	26.4	29.5%
8		179.4	30.4	50.9%	35.7	39.8%
9		179.5	32.4	54.2%	13.2	14.7%
10	(TMP)MoN	200	41.9	57.7%	--	--
11		200	44.7	65.7%	--	--
12		200	46	63.3%	--	--
13	(TMP)$MoCl_2$	200	42	58%	--	--
14[b]	(TMP)MoN	13800	98	2%	--	--
15[c]	(TMP)MoN	100	0.6	2%	--	--
16[d]	(TMP)MoN	140	26	56%	--	--
17[e]	(TMP)MoN	200	36	54%	--	--
18[f]	(TMP)MoN	200	31	62%	--	--
19[g]	(TMP)MoN	210	33	48%	--	--

Table S1: Data from individual catalytic runs. Entries where H_2 was not quantified are left blank with '--'. A) Yield based on SmI_2. B) ROH = H_2O. C) Argon atmosphere. D) $^{15}N_2$ atmosphere. E) 30 equivalents of ammonia added to reaction mixture to check for product inhibition. F) Baseline for mercury drop test, ½ reaction mixture used to quantify NH_3 yield. G) Mercury drop test on other ½ solution from entry 18. NH_3 is reported as additional yield beyond that reported in entry 18.

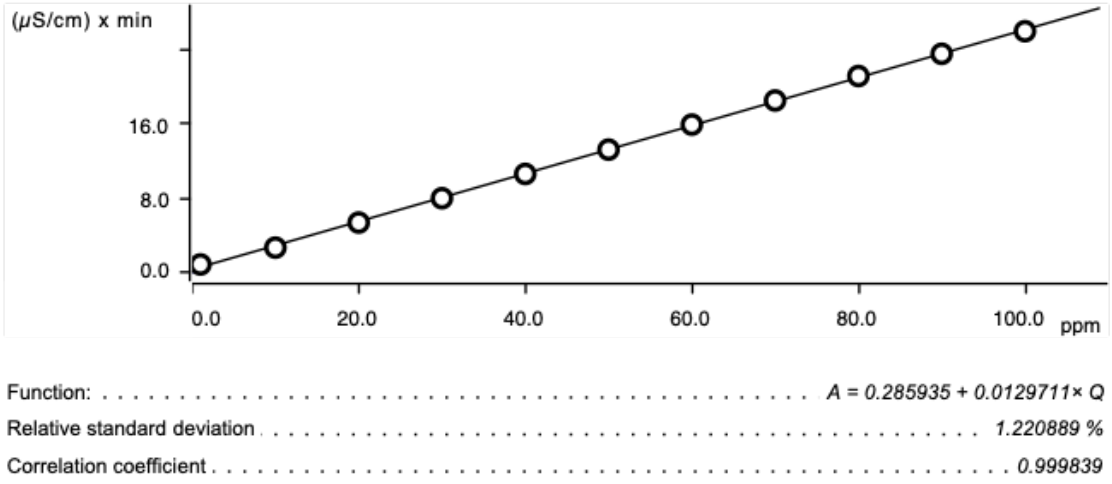

Figure S44: Calibration curve for NH_4^+ quantification by IC.

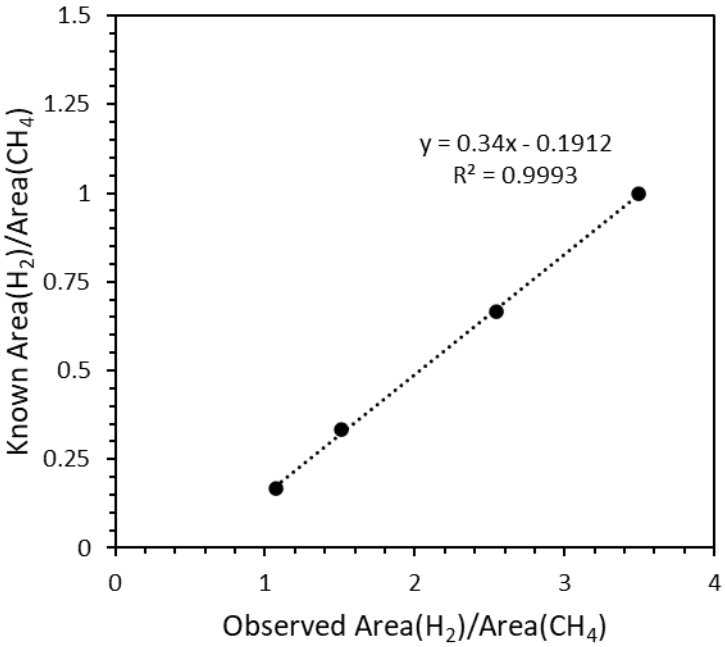

Figure S45: Calibration curve for H_2 quantification by GC.

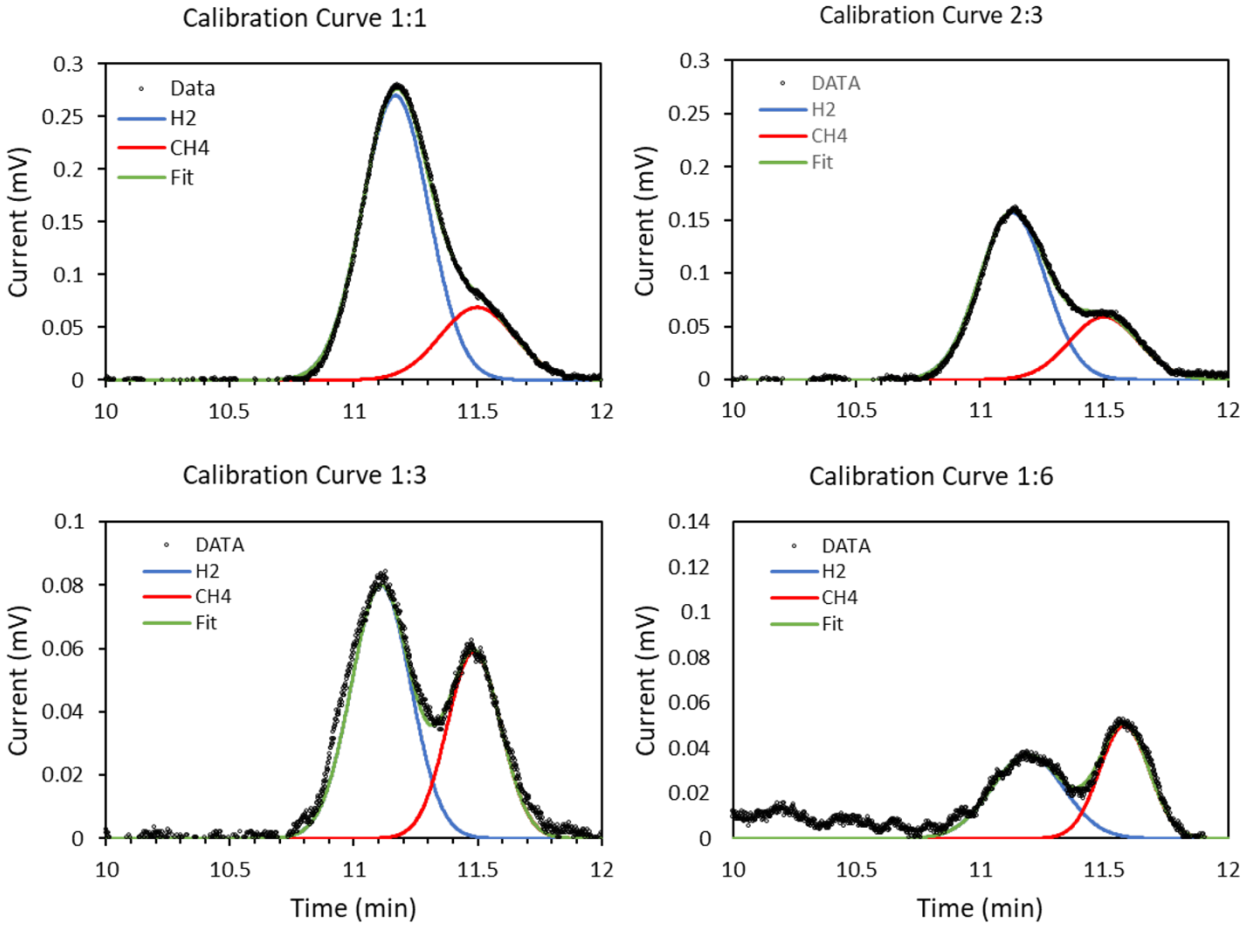

Figure S46: GC data for the H_2 quantification calibration curve overlayed with the gaussian fits.

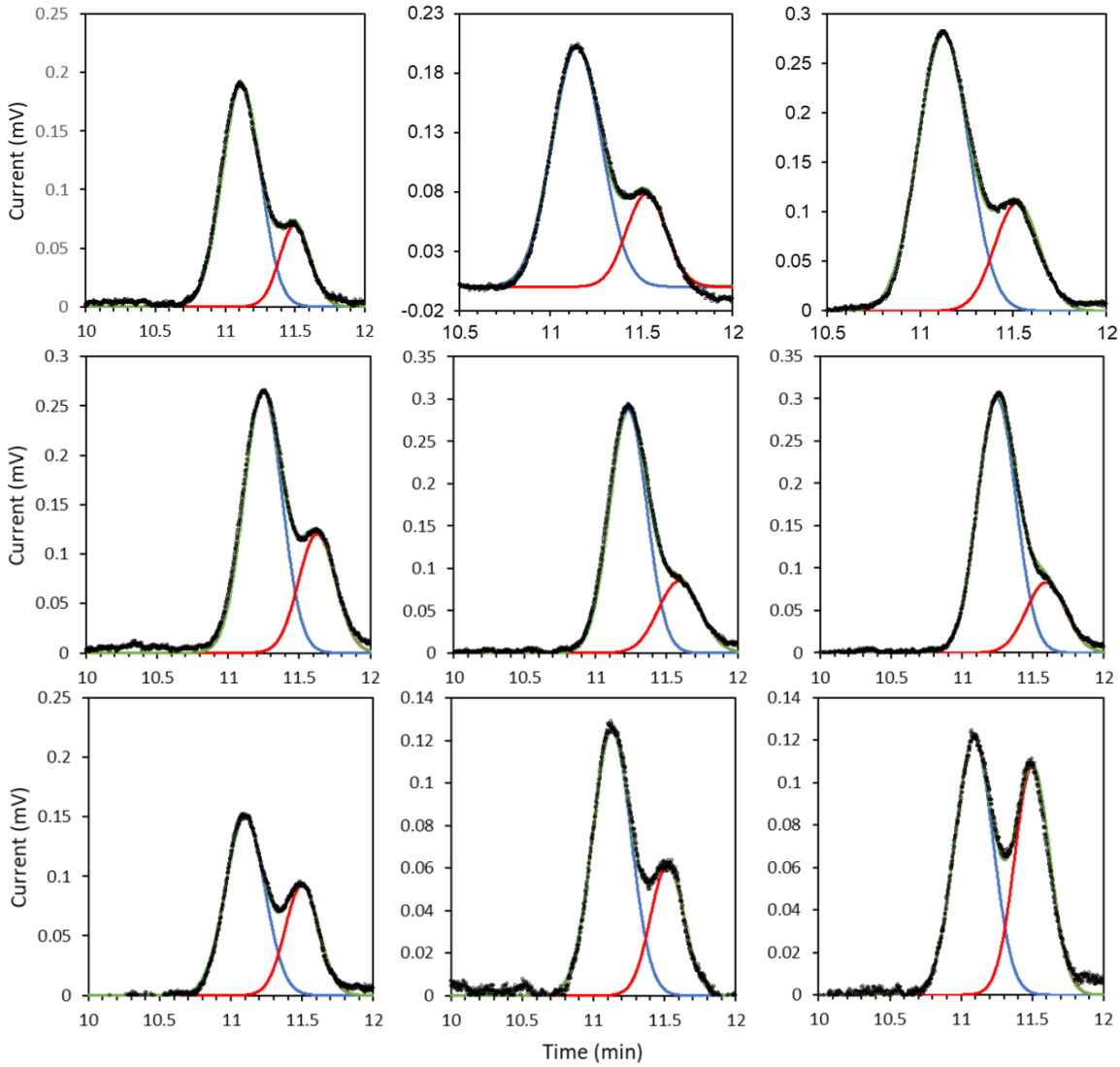

Figure S47: GC data for the H_2 quantification in catalytic runs with **1** (top), **2** (middle), and **3** (bottom) overlayed with the gaussian fits.

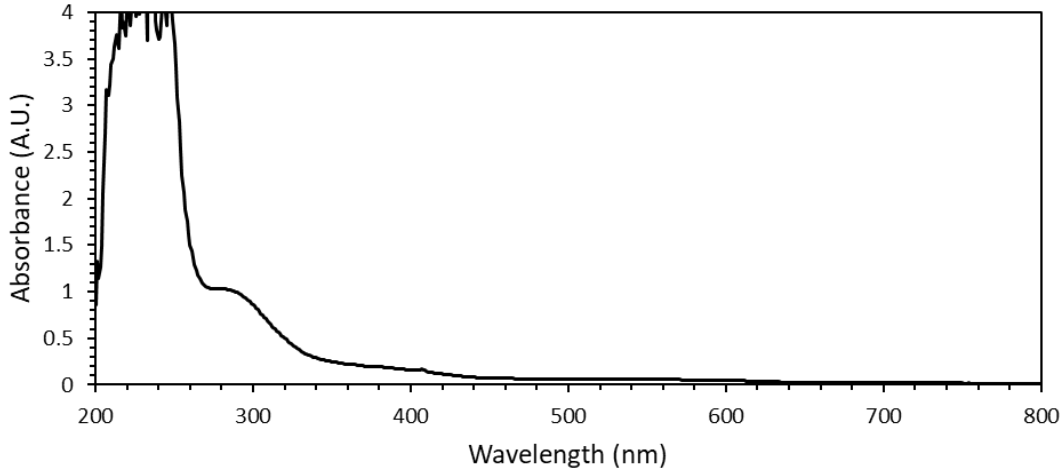

Figure S48: UV-visible spectrum of the reaction mixture post catalysis (Entry 14 in Table S1).

(TMP)MoN-H BDFE Determination

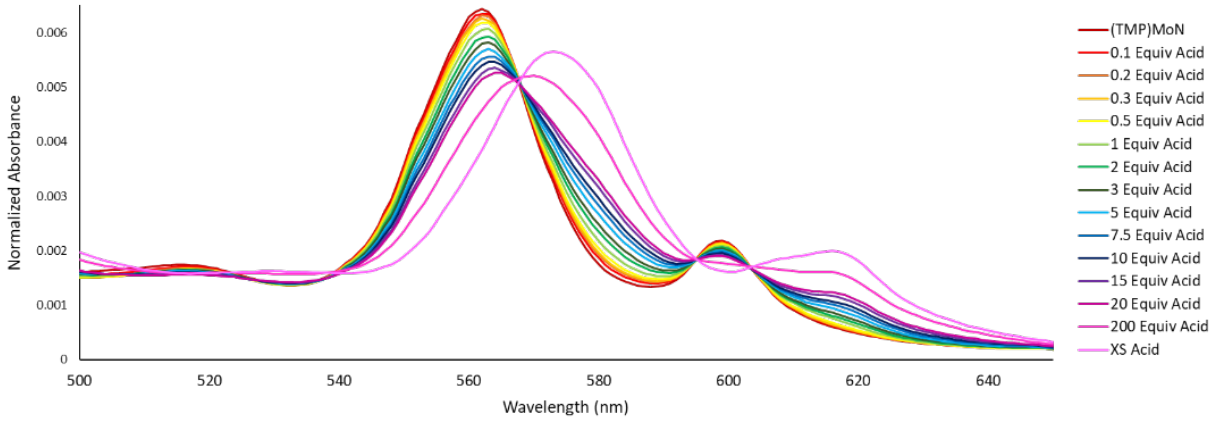

Figure S49: UV-Visible absorption spectrum of the pK_a titration of **3** with [Py-H][OTf] in THF. Absorbances have been corrected for change in concentration as aliquots of acid were added. The final trace was driven to completion by the addition of an excess of [Ph_2NH_2][OTf].

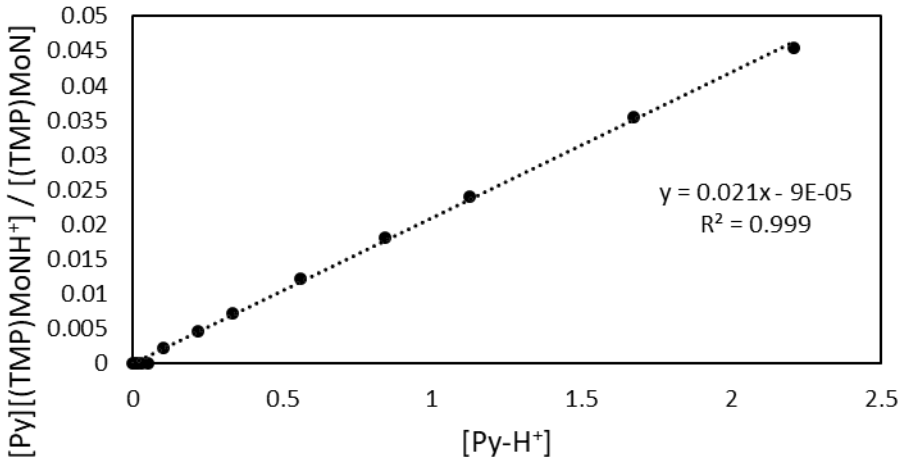

Figure S50: A plot of the concentrations at various points in the titration as determined by the relative absorbance between the starting (TMP)MoN and the fully protonated (TMP)MoNH$^+$. Relative concentrations of each complex were determined for each step in the titration by the average of individual results across the 540 to 650 nm range. The K_{eq} is determined for the equilibrium between the acid and (TMP)MoN using the slope of this plot. With the K_{eq} and the pK_a of pyridine in THF (5.5), the pK_a of (TMP)MoN is determined to be 3.8.

$$K_{\mathrm{eq}} = 10^{\Delta \mathrm{p}K_a}$$

$$\log(K_{eq}) + \mathrm{p}K_{\mathrm{a}}\ of\ [PyH]^+ = \mathrm{p}K_{\mathrm{a}}\ of\ \mathbf{3}$$

$$\log(0.021) + 5.5 = \mathrm{p}K_{\mathrm{a}}\ of\ \mathbf{3}$$

$$\mathrm{p}K_{\mathrm{a}}\ of\ \mathbf{3} = 3.8$$

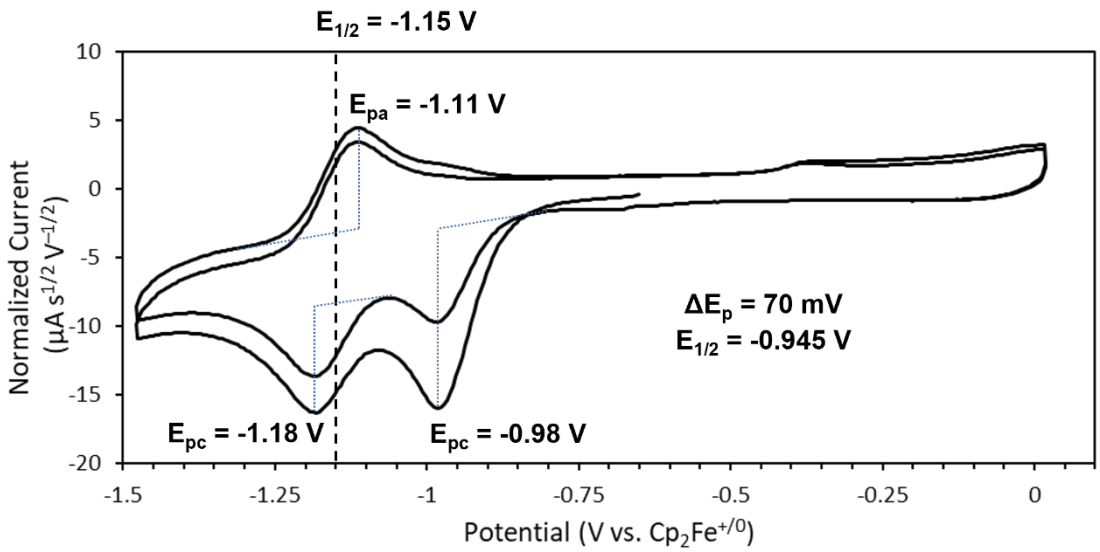

Figure S51: Cyclic voltammogram of **3** with 1 equivalent triflic acid at a scan rate of 500 mV/s. OCP = −0.25 V vs $Fc^{+/0}$. Peak-to-peak separation is determined for the reversible $TMP^{0/\cdot-}$ couple at −1.15 V, and this is used to estimate the $E_{1/2}$ of the first reduction at −0.945 V vs $Fc^{+/0}$.

Using C_G reported by the Mayer group,[6] we estimate the (TMP)Mo=N-H BDFE at 43 kcal/mol.

$$BDFE = 23.06E° + 1.37\mathrm{p}Ka + C_G$$

$$BDFE = 23.06(-0.945) + 1.37(3.8) + 59.9$$

$$BDFE = 43.3 \text{ kcal/mol}$$

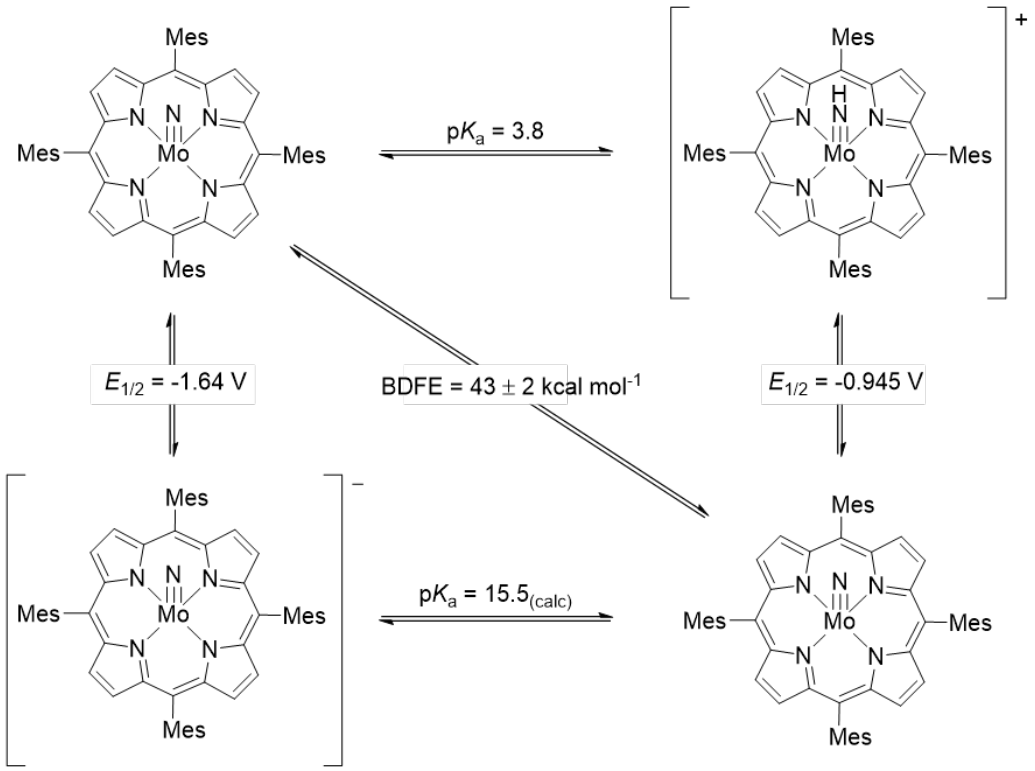

Figure S52: Square scheme of the molybdenum nitride to imido transformation.

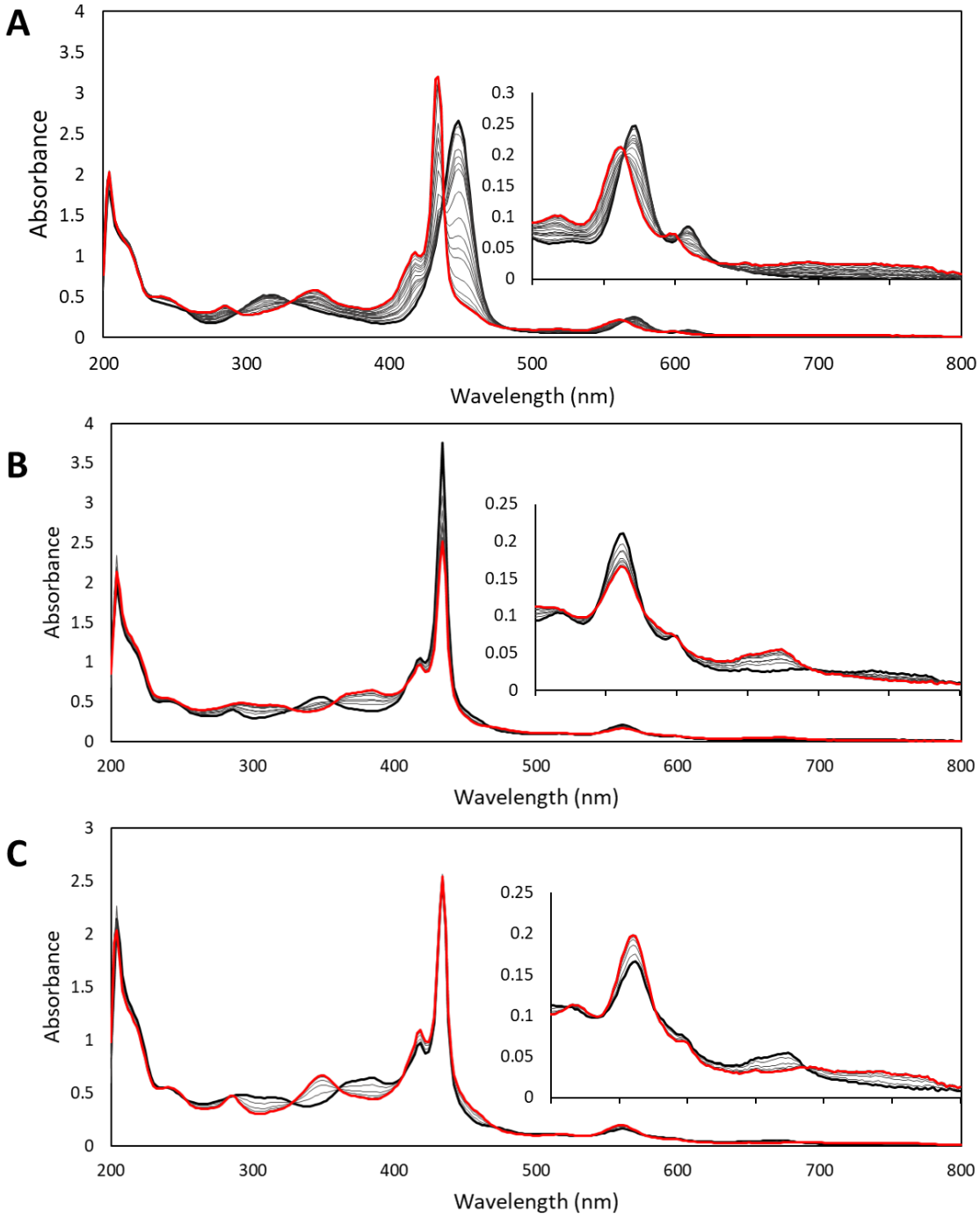

Figure S53: UV-SEC traces of **3** in the presence of 1 equivalent of TfOH in an OTTLE cell. CPE was performed at each potential for 1 minute, collecting a visible spectrum every 15 s. **A)** Potential was varied from −0.7 V (black trace) to −1 V vs Fc^+/Fc (red trace) by steps of 0.1 V. Shows reconversion to the parent nitride, presumably through bimolecular elimination of H_2. **B)** Potential was varied from −1 V (black trace) to −1.3 V vs Fc^+/Fc (red trace) by steps of 0.1 V. **C)** CPE at −0.8 V vs Fc^+/Fc for 1 minute (black trace t = 0, red trace t = 1).

Computational Details

DFT calculations were performed using ORCA version 5.0.3. Structures were optimized using the B3LYP functional and SARC-def2-TZVP basis set, and minima were confirmed by the presence of all real frequencies. Solvation energies were then computed for the minimized structures. Example input files for the geometry optimization/frequency calculation and solvation are shown below.

```
! B3LYP RIJCOSX D3BJ ZORA ZORA-def2-TZVP SARC/J UKS
! TightSCF TightOpt NumFreq NormalPrint

%basis
NewGTO Mo "SARC-ZORA-TZVP" end
end

%output
Print [ P_Basis ] 2
Print [ P_MOs ] 1
end

%pal nproc 20
end

*xyzfile 0 2 name.xyz
```

```
! B3LYP RIJCOSX D3BJ ZORA ZORA-def2-TZVP SARC/J UKS NBO
! TightSCF NormalPrint CPCM(THF)

%basis
NewGTO Mo "SARC-ZORA-TZVP" end
end

%pal nproc 20
end

*xyzfile 0 2 name.xyz
```

Compound	Final Single Point Energy (gas)	*G*-E(el) (gas)	Final Single Point Energy (solv)	G_{solv}	*G* total (Hartree)	*G* total (kcal/mol)
TMPMoN	-6528.55077 NA	0.84379112 NA	NA -6528.585097	-0.03433	-6527.741306	-4096216.419
TMPMoNH LS	-6529.141286 NA	0.85409549 NA	NA -6529.172012	-0.03073	-6528.317916	-4096578.247
TMPMoNH HS	-6529.131275 NA	0.85012249 NA	NA -6529.160331	-0.02906	-6528.310209	-4096573.411
TEMPO	-484.0062454 NA	0.22564235 NA	NA -484.0158039	-0.00956	-483.7901616	-303582.6805
TEMPOH	-484.616424 NA	0.23744005 NA	NA -484.6239649	-0.00754	-484.3865248	-303956.9038
Co(III,N)+	-2151.552417 NA	0.27995219 NA	NA -2151.616663	-0.06425	-2151.336711	-1349983.148
Co(II,NH)+	-2152.110791 NA	0.28923542 NA	NA -2152.190211	-0.07942	-2151.900975	-1350337.229
CoCp*2-H+	-2180.255216 NA	0.40471947 NA	NA -2180.317951	-0.06274	-2179.913232	-1367915.172
CoCp*2+	-2179.704686 NA	0.39885131 NA	NA -2179.767528	-0.06284	-2179.368677	-1367573.459

Table S2. Computed gas-phase and solvent-corrected free energies for **3**, the (TMP)Mo^{IV} imido complex, and H-atom donors/acceptors.

	Reactants	Products
	TEMPO	TEMPOH
	TMPMoNH HS	TMPMoN
G	-7012.10037	-7012.12783
Δ*G* (Ha)	-0.0274601	
kcal/mol	-17.23146014	
BDFE	48.26853986	

	Reactants	Products
	TEMPO	TEMPOH
	TMPMoNH LS	TMPMoN
G	-7012.1081	-7012.1278
Δ*G* (Ha)	-0.019752745	
kcal/mol	-12.39502555	
BDFE	53.10497445	

	Reactants	Products
	$Co^{III}Cp^*_2$	$CoCp^*_2$-H^+
	TMPMoNH HS	TMPMoN
G	-8707.67889	-8707.65454
Δ*G* (Ha)	0.024348212	
kcal/mol	15.27872196	
BDFE	44.27872196	

	Reactants	Products
	$Co^{III}Cp^*_2$	$CoCp^*_2$-H^+
	TMPMoNH LS	TMPMoN
G	-8707.6866	-8707.6545
Δ*G* (Ha)	0.032055567	
kcal/mol	20.11515654	
BDFE	49.11515654	

	Reactants	Products
	$Co(III,N)^+$	$Co(II,NH)^+$
	TMPMoNH HS	TMPMoN
G	-8679.64692	-8679.6423
Δ*G* (Ha)	0.004638596	
kcal/mol	2.910760581	
BDFE	41.81076058	

	Reactants	Products
	$Co(III,N)^+$	Co(II,NH)+
	TMPMoNH LS	TMPMoN
G	-8679.6546	-8679.6423
Δ*G* (Ha)	0.012345951	
kcal/mol	7.747195165	
BDFE	46.64719516	

Table S3-S8: Conversion of calculated energies into BDFEs using Equations below.

$$(\mathrm{TMP})\mathrm{Mo} = \mathrm{NH} + \mathrm{A}^{\cdot} \xrightarrow{\Delta G^\circ} (\mathrm{TMP})\mathrm{Mo} \equiv \mathrm{N} + \mathrm{A} - \mathrm{H}$$

$$\mathrm{BDFE(NH)} = \Delta G^\circ(\mathrm{NH}) + \mathrm{BDFE}_{(\mathrm{expt})}(\text{A-H})$$

H-Atom Acceptor	Acceptor Experimental BDFE (kcal/mol)	Calculated Imido BDFE (low-spin) (kcal/mol)	Calculated Imido BDFE (high-spin) (kcal/mol)
TEMPO/TEMPOH	65.5[7]	53.1	48.3
$Co^{III}Cp^*_2/Co^{II}Cp^*(C_5Me_5H)$	29[8]	49.1	44.3
$Co(III, N)^+/Co(II, NH)^+$	38.9[9]	46.6	41.8

Table S9: Computed molybdenum imido N-H BDFEs with reference to experimental H-atom transfer reagents. BDFEs were computed for both high and low spin (TMP)Mo=NH configurations.

X-Ray Crystallographic Data

(TMP)MoO (1)

Low-temperature diffraction data (ω-scans) were collected on a Rigaku MicroMax-007HF diffractometer coupled to a Dectris Pilatus3R detector with Mo Kα (λ = 0.71073 Å) for the structure of 007a-22176. The diffraction images were processed and scaled using Rigaku Oxford Diffraction software (CrysAlisPro; Rigaku OD: The Woodlands, TX, 2015). The structure was solved with SHELXT and was refined against F^2 on all data by full-matrix least squares with SHELXL.[10] All non-hydrogen atoms were refined anisotropically. Hydrogen atoms were first found in the difference map, then generated geometrically and refined as riding atoms. The isotropic displacement parameters of hydrogen atoms were fixed to 1.2 times the U value of the atoms to which they are linked for CH groups and to 1.5 times the U value of the atoms to which they are linked for CH_3 groups. The unit cell contains approximately 69 electrons that were not well modeled by solvents added to the Q-peaks. To model the Q-peaks with a hexagon geometry as toluene molecules, it was necessary to constrain their geometries using optimized coordinates, as described by Ilia Guzei, using a toluene fragment from their library.[11] The occupancy of each was fixed at 0.25. A similarity restraint was used on the displacement parameters of all disordered atoms within the toluene model. This did not account for all of the unmodeled electron density in the structure, and from the ^{1}H NMR spectrum, it is probable that there is a fractional amount of pentane in the lattice, but these positions were not located in the difference map.

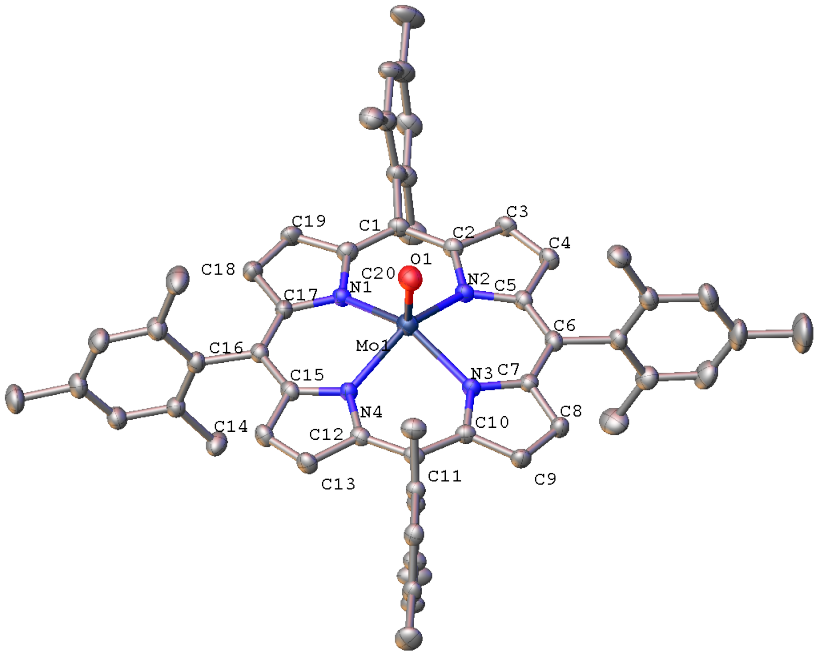

Figure S54: X-ray crystal structure of **1** with partial numbering shown for the atoms within the macrocycle ring. Hydrogen atoms and a disordered molecule of toluene omitted for clarity. Ellipsoids shown at 50% probability.

basis	Δ_{ip}	δ_{ip}	B_{2g}	B_{1g}	$E_u(x)$	$E_u(y)$	A_{1g}	A_{2g}
min.	0.12	0.00	-0.03	0.02	0.00	-0.02	0.11	0.00
ext.	0.13	0.00	-0.03	0.02	0.00	-0.02	0.11	0.00
			0.01	0.01	0.00	0.00	-0.05	0.00
total	0.13	0.00	-0.03	0.02	0.00	-0.02	0.11	0.00
			0.01	0.01	0.00	0.00	-0.05	0.00
			0.00	0.01	0.00	0.00	0.03	0.00
			0.01	0.00	0.00	0.00	0.00	0.00
			0.00	0.00	0.00	0.00	0.00	0.00
			0.01	-0.01	0.00	0.01	0.00	
					0.00	0.00		
					0.00	0.00		
					0.00	0.00		
					-0.01	0.00		
					-0.01	0.00		
comp.	0.13	0.00	0.04	0.02	0.01	0.02	0.12	0.01

basis	Δ_{oop}	δ_{oop}	B_{2u}	B_{1u}	A_{2u}	$E_g(x)$	$E_g(y)$	A_{1u}
min.	0.44	0.00	0.11	-0.29	0.31	0.00	-0.04	0.01
ext.	0.44	0.00	0.11	-0.29	0.31	0.00	-0.04	0.01
			-0.02	0.00	-0.05	0.02	0.00	0.00
total	0.44	0.00	0.11	-0.29	0.31	0.00	-0.04	0.01
			-0.02	0.00	-0.05	0.02	0.00	0.00
			0.00	-0.01	0.01	0.01	0.00	
						0.00	0.00	
						0.00	0.00	
comp.	0.44	0.00	0.11	0.29	0.31	0.02	0.04	0.01

Table S10. Summary of the NSD (in Å) for 1 generated by the porphyrin NSD online tool – https://www.sengegroup.eu/nsd.[12]

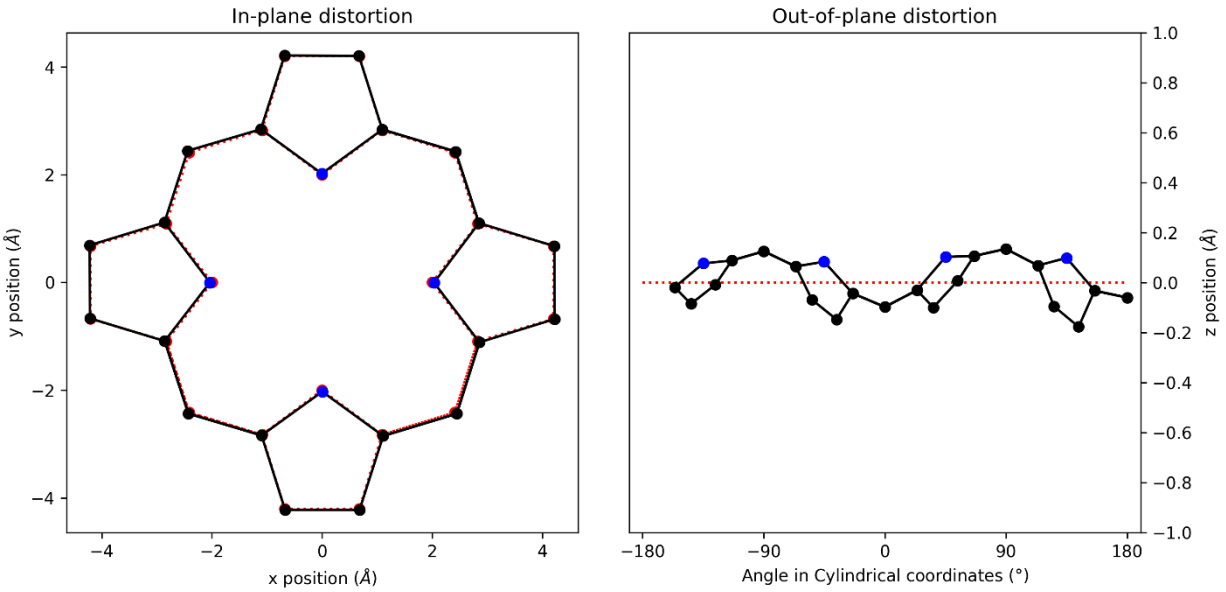

Figure S55. (A) out-of-plane and (B) in-plane skeletal plots of the porphyrin core. **1** is represented in black (C) and blue (N), with the reference structure, (TPP)Cu, in red dotted lines.[12]

Bond Distances, Bond Angles, Atom Displacements	**Mean Value (standard error)**	**Units**
$N–C_a$	1.378(5)	(Å)
$C_a–C_b$	1.437(6)	(Å)
$C_a–C_m$	1.396(7)	(Å)
$C_b–C_b$	1.356(2)	(Å)
$\angle C_aC_bC_b$	107.3(2)	(°)
$\angle NC_aC_b$	109.4(3)	(°)
$\angle NC_aC_m$	126.1(4)	(°)
$\angle C_aNC_a$	106.7(3)	(°)
$\angle C_mC_aC_b$	124.5(4)	(°)
$\angle C_aC_mC_a$	124.41(16)	(°)
Δ24	0.08	(Å)
ΔN	0.091(11)	(Å)
ΔC_a	0.06(3)	(Å)
ΔC_b	0.09(6)	(Å)
ΔC_m	0.1(3)	(Å)
∠ pyrrole tilt	5.6(9)	(°)
N···N dist (adj)	2.87(4)	(Å)
N···N dist (opp)	4.059(11)	(Å)

Table S11. Bond distances, angles and deviations from planarity for **1** generated from NSD.[12]

Table S12. Crystal data and structure refinement for (TMP)MoO.

Identification code	007a-22176	
CCDC code	2221212	
Empirical formula	C59.50 H56 Mo N4 O	
Formula weight	939.02	
Temperature	93(2) K	
Wavelength	1.54184 Å	
Crystal system	Triclinic	
Space group	P-1	
Unit cell dimensions	a = 11.8219(4) Å	α= 93.563(3)°.
	b = 13.2826(4) Å	β= 98.612(3)°.
	c = 16.6908(5) Å	γ = 99.221(3)°.
Volume	2547.86(14) $Å^3$	
Z	2	
Density (calculated)	1.224 g/cm^3	
Absorption coefficient	2.432 mm^{-1}	
F(000)	982	
Crystal size	0.100 x 0.020 x 0.010 mm^3	
Crystal color and habit	Purple Block	
Diffractometer	dtrek-CrysAlisPro-abstract goniometer imported rigaku-d*trek images	
Theta range for data collection	2.688 to 66.600°.	
Index ranges	-14<=h<=14, -15<=k<=15, -19<=l<=19	
Reflections collected	94134	
Independent reflections	8891 [R(int) = 0.0729]	
Observed reflections (I > 2sigma(I))	7876	
Completeness to theta = 66.600°	98.8 %	
Absorption correction	Semi-empirical from equivalents	
Max. and min. transmission	1.00000 and 0.73172	
Solution method	?	
Refinement method	SHELXL-2014/7 (Sheldrick, 2014)	
Data / restraints / parameters	8891 / 84 / 667	
Goodness-of-fit on F^2	1.057	
Final R indices [I>2sigma(I)]	R1 = 0.0639, wR2 = 0.1897	
R indices (all data)	R1 = 0.0709, wR2 = 0.1955	
Extinction coefficient	n/a	
Largest diff. peak and hole	1.063 and -1.156 e.$Å^{-3}$	

(TMP)$MoCl_2$ (2)

Low-temperature diffraction data (ω-scans) were collected on a Rigaku MicroMax-007HF diffractometer coupled to a Dectris Pilatus3R detector with Mo Kα (λ = 0.71073 Å) for the structure of 007a-22176. The diffraction images were processed and scaled using Rigaku Oxford Diffraction software (CrysAlisPro; Rigaku OD: The Woodlands, TX, 2015). The structure was solved with SHELXT and was refined against F^2 on all data by full-matrix least squares with SHELXL.[10] All non-hydrogen atoms were refined anisotropically. Hydrogen atoms were first found in the difference map, then generated geometrically and refined as riding atoms. The isotropic displacement parameters of hydrogen atoms were fixed to 1.2 times the U value of the atoms to which they are linked for CH groups and to 1.5 times the U value of the atoms to which they are linked for CH_3 groups. While most of the protons on the methyl groups were allowed to freely rotate, the protons on C32 and C26 prevented the structure from converging. Consequently, free C-C rotation was removed from the refined model of these atoms. In modeling the disorder of the toluene molecules, it was necessary to first refine the site occupancies of the C atoms as fixed values of 0.5. The aromatic C-C and C-methyl C bonds of both toluene molecules were restrained to be similar. The atomic displacement parameters of C33A and C39B were restrained to be similar. Next, the site occupancies of the toluene C's were freely refined and subsequently restrained to values of 0.4/0.6.

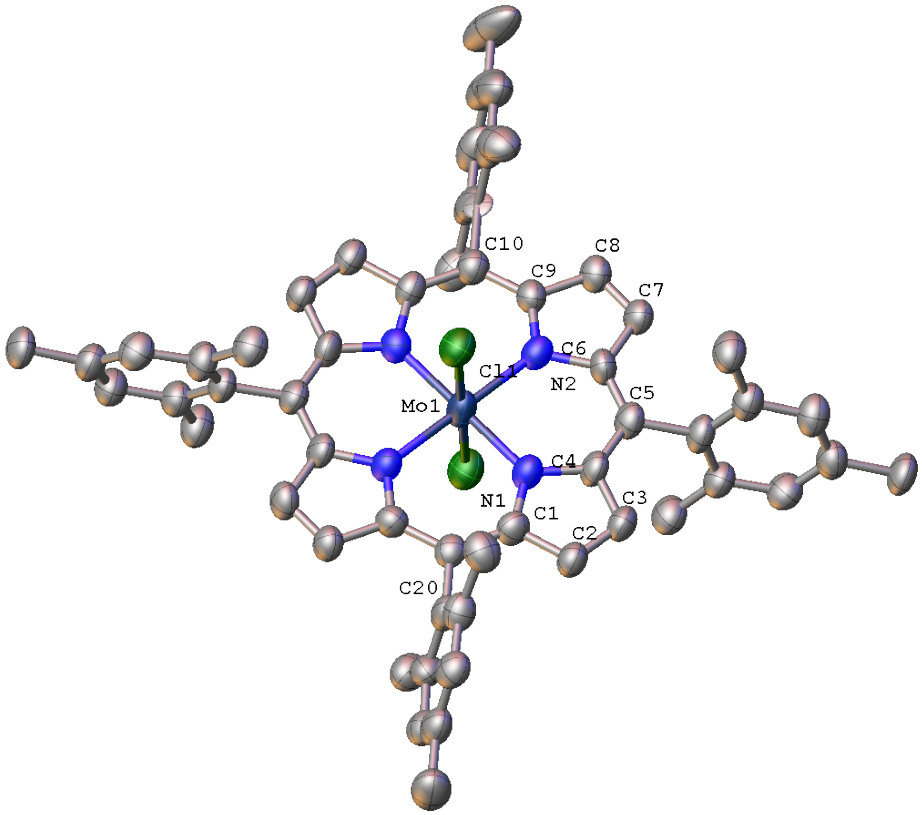

Figure S56: X-ray crystal structure of **2** with partial numbering shown for the atoms within the macrocycle that are included in the asymmetric unit. Hydrogen atoms and a disordered molecule of toluene omitted for clarity. Ellipsoids shown at 50% probability.

basis	Δ_{ip}	δ_{ip}	B_{2g}	B_{1g}	$E_u(x)$	$E_u(y)$	A_{1g}	A_{2g}
min.	0.24	0.00	-0.01	0.00	0.00	0.00	0.24	0.00
ext.	0.25	0.00	-0.01	0.00	0.00	0.00	0.24	0.00
			0.01	0.00	0.01	-0.01	-0.05	0.00
total	0.25	0.00	-0.01	0.00	0.00	0.00	0.24	0.00
			0.01	0.00	0.01	-0.01	-0.05	0.00
			-0.01	0.00	0.00	0.00	0.04	0.00
			0.00	0.00	-0.01	0.01	0.01	0.00
			0.00	0.00	0.00	0.00	-0.02	0.00
			0.00	0.00	0.00	0.00	0.01	
					0.01	-0.01		
					-0.01	0.01		
					0.00	0.00		
					0.00	0.00		
					0.00	0.00		
comp.	0.25	0.00	0.02	0.00	0.02	0.02	0.25	0.00

basis	Δ_{oop}	δ_{oop}	B_{2u}	B_{1u}	A_{2u}	$E_g(x)$	$E_g(y)$	A_{1u}
min.	0.02	0.00	0.01	0.00	0.00	0.01	-0.01	-0.01
ext.	0.10	0.00	0.01	0.00	0.00	0.02	-0.02	-0.01
			-0.01	0.00	0.00	0.07	-0.07	0.00
total	0.11	0.00	0.01	0.00	0.00	0.02	-0.02	-0.01
			-0.01	0.00	0.00	0.07	-0.07	0.00
			0.00	0.00	0.00	0.02	-0.02	
						0.00	0.00	
						0.00	0.00	
comp.	0.11	0.00	0.01	0.00	0.00	0.08	0.08	0.01

Table S13. Summary of the NSD (in Å) for 1 generated by the porphyrin NSD online tool – https://www.sengegroup.eu/nsd.[12]

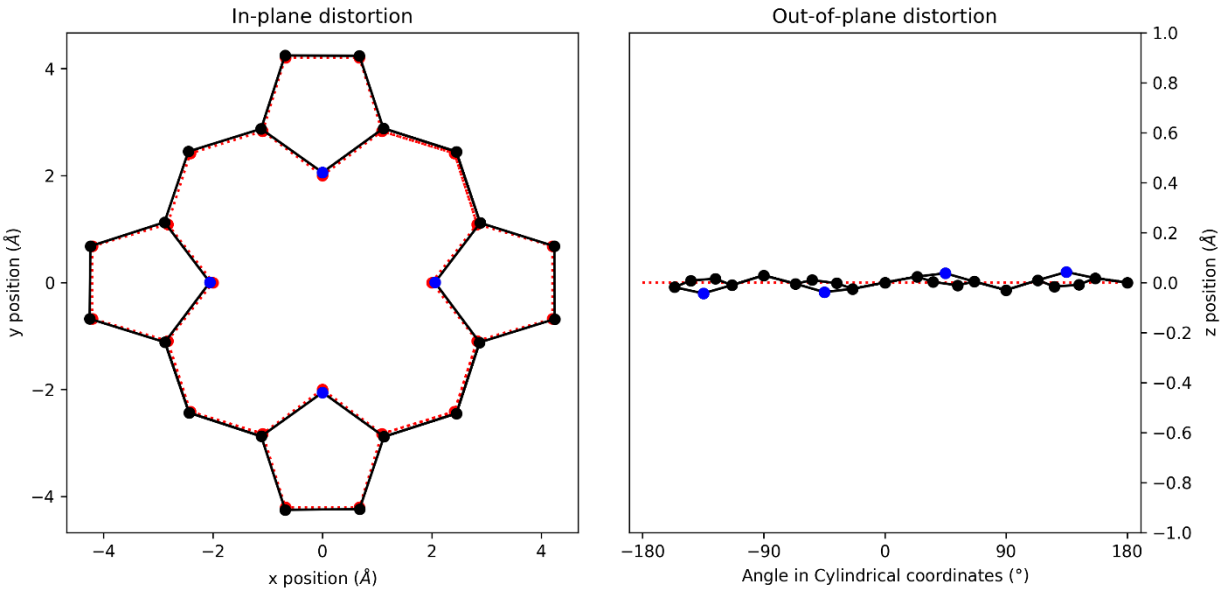

Figure S57. (A) out-of-plane and (B) in-plane skeletal plots of the porphyrin core. **1** is represented in black (C) and blue (N), with the reference structure, (TPP)Cu, in red dotted lines.[12]

Bond Distances, Bond Angles, Atom Displacements	**Mean Value (standard error)**	**Units**
$N–C_a$	1.389(4)	(Å)
$C_a–C_b$	1.433(8)	(Å)
$C_a–C_m$	1.395(4)	(Å)
$C_b–C_b$	1.36(2)	(Å)
$\angle C_aC_bC_b$	107.8(6)	(°)
$\angle NC_aC_b$	108.5(2)	(°)
$\angle NC_aC_m$	125.6(4)	(°)
$\angle C_aNC_a$	107.34(4)	(°)
$\angle C_mC_aC_b$	125.9(4)	(°)
$\angle C_aC_mC_a$	126.2(5)	(°)
Δ24	0.0171	(Å)
ΔN	0.04(3)	(Å)
ΔC_a	0.014(8)	(Å)
ΔC_b	0.009(5)	(Å)
ΔC_m	0.015(15)	(Å)
∠ pyrrole tilt	1.25(12)	(°)
N···N dist (adj)	2.908(3)	(Å)
N···N dist (opp)	4.1131(4)	(Å)

Table S14. Bond distances, angles and deviations from planarity for **1** generated from NSD.[12]

Table S15. Crystal data and structure refinement for **2**.

Identification code	007a-21088	
CCDC code	2221213	
Empirical formula	C70 H68 Cl2 Mo N4	
Formula weight	1132.12	
Temperature	223(2) K	
Wavelength	1.54184 Å	
Crystal system	Monoclinic	
Space group	C2/c	
Unit cell dimensions	a = 19.8644(10) Å	α= 90°.
	b = 25.0963(9) Å	β= 105.033(7)°.
	c = 11.9054(9) Å	γ = 90°.
Volume	5732.0(6) $Å^3$	
Z	4	
Density (calculated)	1.312 g/cm^3	
Absorption coefficient	3.078 mm^{-1}	
F(000)	2368	
Crystal size	0.100 x 0.100 x 0.050 mm^3	
Crystal color and habit	purple block	
Diffractometer	dtrek-CrysAlisPro-abstract goniometer imported rigaku-d*trek images	
Theta range for data collection	2.899 to 67.068°.	
Index ranges	-23<=h<=23, -29<=k<=29, -14<=l<=14	
Reflections collected	100161	
Independent reflections	5112 [R(int) = 0.2759]	
Observed reflections (I > 2sigma(I))	2794	
Completeness to theta = 67.068°	99.8 %	
Absorption correction	Semi-empirical from equivalents	
Max. and min. transmission	1.00000 and 0.86775	
Solution method	SHELXT	
Refinement method	SHELXL-2014/7 (Sheldrick, 2014)	
Data / restraints / parameters	5112 / 283 / 423	
Goodness-of-fit on F^2	1.033	
Final R indices [I>2sigma(I)]	R1 = 0.0974, wR2 = 0.2361	
R indices (all data)	R1 = 0.1622, wR2 = 0.2843	
Extinction coefficient	n/a	
Largest diff. peak and hole	2.335 and -0.847 $e.Å^{-3}$	

References

1 J. S. Lindsey and R. W. Wagner, *J. Org. Chem.,* 1989, **54**, 828-836 (DOI:10.1021/jo00265a021).

2 J. C. Kim, W. S. Rees and V. L. Goedken, *Inorg. Chem.,* 1994, **33**, 3191-3194 (DOI:10.1021/ic00092a030).

3 S. Saba, R. Hernandez, C. C. Choy, K. Carta, Y. Bennett, S. Bondi, S. Kolaj and C. Bennett, *J. Fluorine Chem.,* 2013, **153**, 168-171 (DOI:10.1016/j.jfluchem.2013.05.007).

4 M. Krejčik, M. Daněk and F. Hartl, *Journal of Electroanalytical Chemistry and Interfacial Electrochemistry,* 1991, **317**, 179-187 (DOI:10.1016/0022-0728(91)85012-E).

5 A. J. Kendall, S. I. Johnson, R. M. Bullock and M. T. Mock, *J. Am. Chem. Soc.,* 2018, **140**, 2528-2536 (DOI:10.1021/jacs.7b11132).

6 R. G. Agarwal, S. C. Coste, B. D. Groff, A. M. Heuer, H. Noh, G. A. Parada, C. F. Wise, E. M. Nichols, J. J. Warren and J. M. Mayer, *Chem. Rev.,* 2022, **122**, 1-49 (DOI:10.1021/acs.chemrev.1c00521).

7 C. F. Wise, R. G. Agarwal and J. M. Mayer, *J. Am. Chem. Soc.,* 2020, **142**, 10681-10691 (DOI:10.1021/jacs.0c01032).

8 M. J. Chalkley, P. H. Oyala and J. C. Peters, *J. Am. Chem. Soc.,* 2019, **141**, 4721-4729 (DOI:10.1021/jacs.9b00193).

9 M. J. Chalkley, P. Garrido-Barros and J. C. Peters, *Science,* 2020, **369**, 850-854 (DOI:10.1126/science.abc1607).

10 S. George, *Acta Crystallographica Section A,* 2008, **64**, 112-122 (DOI:10.1107/S0108767307043930).

11 G. Ilia, *Journal of Applied Crystallography,* 2014, **47**, 806-809 (DOI:10.1107/S1600576714004427).

12 C. J. Kingsbury and M. O. Senge, *Coord. Chem. Rev.,* 2021, **431**, 213760 (DOI:10.1016/j.ccr.2020.213760).